bioRxiv preprint doi: https://doi.org/10.1101/2022.12.23.521743; this version posted December 23, 2022. The copyright holder for this preprint (which was not certified by peer review) is the author/funder, who has granted bioRxiv a license to display the preprint in perpetuity. It is made available under aCC-BY-NC 4.0 International license.

How much data do we need? Lower bounds of brain activation states to predict human cognitive ability

Maren H. Wehrheim[a,b], Joshua Faskowitz[c], Olaf Sporns[c], Christian J. Fiebach[a,d], Matthias Kaschube[b,e,1], Kirsten Hilger[a,f,1,*]

[a] Department of Psychology, Goethe University Frankfurt, D-60323 Frankfurt am Main, Germany
[b] Department of Computer Science, Goethe University Frankfurt, D-60325 Frankfurt am Main, Germany
[c] Department of Psychological and Brain Sciences, Indiana University, Bloomington, IN 47405,
[d] Brain Imaging Center, Goethe University, D-60528 Frankfurt am Main, Germany
[e] Frankfurt Institute for Advanced Studies, D-60438 Frankfurt am Main, Germany
[f] Department of Psychology I, Julius Maximilian University, D-97070 Würzburg, Germany

[1] these authors share senior authorship

[*]Corresponding author:
Kirsten Hilger
Address: Marcusstr. 9-11, D-97970 Würzburg, Germany
Phone: +49 931 31-81141
Email: kirsten.hilger@uni-würzburg.de

Author Contributions:
M.W., C.F., M.K., and K.H. conceived of the study. M.W., M.K., and K.H. analyzed the data. J.F. and O.S. preprocessed the HCP data and provided theoretical input during analyses. All authors were involved in the interpretation of results and provided feedback during manuscript preparation.

Competing Interest Statement: The authors declared no potential conflicts of interest with respect to the research, authorship, and/or publication of this article.

Keywords: intelligence, functional connectivity, time-varying connectivity, resting-state fMRI, predictive modelling

This PDF file includes:

Main Text
Figures 1 to 5 (each Figure preferred to be printed in medium size)
Table 1

bioRxiv preprint doi: https://doi.org/10.1101/2022.12.23.521743; this version posted December 23, 2022. The copyright holder for this preprint (which was not certified by peer review) is the author/funder, who has granted bioRxiv a license to display the preprint in perpetuity. It is made available under aCC-BY-NC 4.0 International license.

Abstract

Human functional brain connectivity can be temporally decomposed into states of high and low cofluctuation, defined as coactivation of brain regions over time. Despite their low frequency of occurrence, states of particularly high cofluctuation have been shown to reflect fundamentals of intrinsic functional network architecture (derived from resting-state fMRI) and to be highly subject-specific. However, it is currently unclear whether such network-defining states of high cofluctuation also contribute to individual variations in cognitive abilities – which strongly rely on the interactions among distributed brain regions. By introducing CMEP, an eigenvector-based prediction framework, we show that functional connectivity estimates from as few as 20 temporally separated time frames (< 3% of a 10 min resting-state fMRI scan) are significantly predictive of individual differences in intelligence (N = 281, p < .001). In contrast and against previous expectations, individual's network-defining time frames of particularly high cofluctuation do not achieve significant prediction of intelligence. Multiple functional brain networks contribute to the prediction, and all results replicate in an independent sample (N = 831). Our results suggest that although fundamentals of person-specific functional connectomes can be derived from few time frames of highest brain connectivity, temporally distributed information is necessary to extract information about cognitive abilities from functional connectivity time series. This information, however, is not restricted to specific connectivity states, like network-defining high-cofluctuation states, but rather reflected across the entire length of the brain connectivity time series.

bioRxiv preprint doi: https://doi.org/10.1101/2022.12.23.521743; this version posted December 23, 2022. The copyright holder for this preprint (which was not certified by peer review) is the author/funder, who has granted bioRxiv a license to display the preprint in perpetuity. It is made available under aCC-BY-NC 4.0 International license.

Significance Statement

Neuroimaging has significantly contributed to our understanding about human cognition. Individual differences in cognitive ability can be assessed with intelligence tests and resulting scores predict important life outcomes. Previous research revealed that few states of high brain-wide connectivity determine individuals functional connectomes. We show that these states do not predict intelligence but identify alternative states which contain intelligence-predictive information. These states comprise a minimum of 20 time frames (< 3% of 10 min resting-state fMRI), include a distributed network of brain regions, and their temporal independence is a critical prerequisite. Means to find these states are relevant for future neuroimaging research on complex human traits and the here introduced prediction framework has potential for broad applications across scientific disciplines.

bioRxiv preprint doi: https://doi.org/10.1101/2022.12.23.521743; this version posted December 23, 2022. The copyright holder for this preprint (which was not certified by peer review) is the author/funder, who has granted bioRxiv a license to display the preprint in perpetuity. It is made available under aCC-BY-NC 4.0 International license.

Main Text

Introduction

Humans differ in cognitive ability as assessed by measures of intelligence. Individual differences in intelligence, in turn, are associated with important life outcomes like academic achievement (1), socio-economic status (2), or health (e.g., 3). While intact brain functions are a necessary pre-condition for intelligent behavior and thought, as evidenced by neuropsychological data from lesion studies (e.g., 4), the neurobiological mechanisms underlying individual differences in intelligence are not yet fully understood (e.g., 5, 6). One currently emerging hypothesis is that individual differences in intelligence (or general cognitive ability) are related not only to the structure or function of distinct brain regions, but to their interactions and the information flow between them (e.g., 7, 8; see also 9) – a proposal that is at least partly consistent with psychological theories postulating that general intelligence is the result of the coordination between several fundamental cognitive processes (including, e.g., working memory capacity and mental processing speed; e.g., 10, 11, for review see 12, 13).

In the past few years, abundant functional MRI (fMRI) research has established that the human brain is organized into functionally dissociable large-scale networks (14 - 17), consisting of anatomically distributed brain regions whose activity covaries across time, even in the absence of specific cognitive task demands (task-free or resting-state fMRI). Multiple studies have demonstrated that individual differences in intelligence can be predicted from resting-state functional MRI connectivity (e.g., 18 - 21), so that a link between functional brain network organization and individual differences in general cognitive ability (intelligence) is widely accepted (see also 22, for an overview of network neuroscience studies on intelligence). The exact nature of this relationship, however, remains to be fully understood.

Human network neuroscience studies have commonly relied on the analysis of 'static' intrinsic functional connectivity, which is derived from correlations between the entire BOLD time series of different brain regions (typically assessed with task-free resting-state fMRI measurements of 5 to 10 minutes in length, e.g., 23). Newer methodological advances made it possible to explore functional connectivity as a 'dynamic' property of the human brain (see 24, for an overview) and suggest that individual differences in behavior and cognition may be related to variations of functional connectivity over time (e.g., 8, 25, 26). Most recently, time-resolved analyses of intrinsic functional connectivity have demonstrated that a small fraction of the fMRI BOLD time series is characterized by particularly strong functional interactions between brain regions (27 - 29) and sufficient to account for several fundamental properties of the static network architecture, including the overall (time-averaged) configuration of connectivity patterns and their hierarchical modular structure (30). These 'network-defining' states of high brain-wide cofluctuation (top 5% of the entire timeseries, i.e., 55 out of 1,100 time frames) were suggested to be temporally stable and highly individual-specific (31-33), as subjects can be identified (in the sense of 'network fingerprinting'; cf. 20) significantly better on the basis of these high-connectivity states, compared to the same number of low cofluctuation time frames (30). Following up on these findings, we here explore whether individual differences in general cognitive ability (intelligence) can be predicted from specific states of intrinsic functional brain connectivity, thereby defining 'states' as selections of fMRI time frames characterized by a particular selection criterion (such as strongest vs. weakest brain-wide cofluctuation).

To this end, we investigated the association between general intelligence and different states of intrinsic functional connectivity in a sample of 281 adults for which intelligence test data (Full-Scale Intelligence Quotient, FSIQ, from the Wechsler Abbreviated Scale of Intelligence; WASI; 34) and temporally highly resolved resting-state fMRI data are available (NKI Enhanced Rockland Sample; 35). To increase the robustness of prediction results we developed a cross-validated machine learning-based prediction framework that circumvents the necessity of selecting arbitrary statistical threshold parameters. First, we replicated earlier reports that static (time-averaged) functional connectivity can significantly predict intelligence. We then identified high cofluctuation time frames as described by (30) and replicate their finding that the general structure of static functional connectivity is strongly determined by a small number of such high cofluctuation states. However, intelligence could not be predicted from these 'network-defining' states, nor from an equal number of time frames reflecting particularly low brain-wide cofluctuations. Systematic analyses showed that more independent (i.e., temporally separated) time frames are required to predict intelligence than to recover major characteristics of general functional

bioRxiv preprint doi: https://doi.org/10.1101/2022.12.23.521743; this version posted December 23, 2022. The copyright holder for this preprint (which was not certified by peer review) is the author/funder, who has granted bioRxiv a license to display the preprint in perpetuity. It is made available under aCC-BY-NC 4.0 International license.

network structure. However, given temporal independence, this number can be as low as 20 time frames and appears largely independent of the ability to predict global network features. Finally, multiple functional networks were involved in the prediction, suggesting intelligence as whole-brain phenomenon. All results have been replicated in an independent sample (N = 812, 36).

Results

General cognitive ability was assessed with an established measure of intelligence (FSIQ from the WASI; 34), and descriptive statistics show that the intelligence quotient is normally distributed in our sample of 18 to 84 year old adults (183 females; 98 males; Supplementary Figure S1). Time-resolved functional connectivity between brain regions (network nodes) was extracted from fast-sampling resting-state fMRI data (primary sample: 114 regions, TR = 654ms; replication sample: 100 regions, TR = 720ms; see Methods and Fig. 1a,b). A covariance maximizing eigenvector-based predictive modelling framework (CMEP, see Fig. 2 and Methods for details) was developed and used for all prediction analyses. This machine learning-based prediction framework involves eigenvector-based generation of features from functional brain connections that highly covary with the variable of interest (Fig. 2 a-e), as well as ElasticNet regression and leave-one-out (LOO) cross validation for prediction (Fig. 2f).

Static functional connectivity predicts intelligence. We first used the CMEP prediction framework to replicate previous findings (e.g., 19, 20) that time-averaged ('static') functional connectivity derived from the full fMRI time series (Fig. 1d) significantly predicts intelligence (correlation between predicted and observed intelligence scores: r = .34; prediction error: MAE = 9.84; all p < .001; see Tab. 1). To establish the validity of CMEP, we compared its prediction results with those derived from the most frequently used prediction frameworks (connectome-based predictive modelling, CPM; cf. 20, 37). Prediction performance of CMEP was robustly superior across different cross-validation splits (Fig. 3a) and when substantially reducing the sample size of the training set to only 10% (Fig 3b), while most models produced similar results when trained on one sample and tested on a new sample (Fig. 3c). See Supplementary Fig. S2 for similar robustness results in the replication sample.

Network-defining states of highest and lowest cofluctuation are not sufficient to predict intelligence. To test whether intelligence could be predicted from 'network-defining' states of highest cofluctuation, we followed the approach introduced by (30) of analyzing only 5% of the dynamic (time-resolved) functional connectivity time series. First, we operationalized the instantaneous strength of brain-wide (global) connectivity as the root-sum-square (RSS) over the cofluctuation between all pairs of nodes (brain regions), independently for each time frame; see Fig. 1b-e). We then selected the 44 time frames corresponding to the 5% highest global cofluctuation frames (HiCo; Fig. 1e red), as well as in an independent analysis the 5% time frames with lowest global cofluctuation (LoCo; Fig. 1e blue). Pearson correlation between the static connectivity matrix (average across all time frames) and the connectivity matrices constructed from only these selections of time frames (Fig. 1f) demonstrated high reconstruction similarity, with on average r = .78 (p < .001) and r = .41 (p < .001), respectively, for high and low cofluctuation states (Tab. 1, Fig. 4a). This replicates the previous finding that an individual's static functional connectome can be well approximated based on just a few time frames of highest cofluctuation (30), thus providing an important precondition for all subsequent analyses.

Next, we tested whether these states of highest cofluctuation are predictive of individual differences in intelligence. However, this was not the case (r = .13, MAE = 10.63, all p > .05). Further, the prediction performance was not significantly different from states of lowest cofluctuation (r = .11, MAE = 10.40, all p > .05; see Tab. 1; Fig. 4b, red and blue). Comparably low prediction performance was also evident when using an alternative prediction model (CPM; Fig. S3). These results suggest that reconstruction similarity (see previous paragraph) is not a faithful indicator for the ability to extract information about individual differences in cognitive ability from brain connectivity states, and that the ability to predict intelligence depends on a richer set of features than that required for approximating global properties of network structure (Fig. 4a,b).

Notably, these network-defining states of highest and lowest cofluctuation contain a comparably large number of temporally adjacent time frames, which are highly correlated in their activity patterns. To test

bioRxiv preprint doi: https://doi.org/10.1101/2022.12.23.521743; this version posted December 23, 2022. The copyright holder for this preprint (which was not certified by peer review) is the author/funder, who has granted bioRxiv a license to display the preprint in perpetuity. It is made available under aCC-BY-NC 4.0 International license.

whether the low prediction performance of highest and lowest cofluctuation states is due to the small number of temporally independent data points contained in these selections, we next selected only the individual-specific maxima/minima from the previously examined states of highest/lowest cofluctuation, respectively (Fig. 1e; maxima: MxCo pink; minima: MnCo light blue). This strongly reduces the amount of time frames (MxCo; 7-14 TFs, mean: 8.25; MnCo; 6-17 TFs, mean: 10.72), but ensures their temporal separation. Notably, neither reconstruction similarity nor prediction performance decreased markedly (MxCo: reconstruction similarity r = .77, p < .001; intelligence prediction r = .09, MAE = 10.65, all p > .05; MnCo: reconstruction similarity r = .32, p < 001; intelligence prediction r = .04, MAE = 10.57, all p > .05; Tab. 1; Fig. 4a,b). The same results were observed when using alternative prediction models, but CMEP provides the highest robustness of results (Fig. S3). Together, these analyses suggest that the low predictive power of connectivity states of highest/lowest cofluctuation for intelligence is most likely due to the small amount of independent information included in these selections of temporally adjacent time frames.

A small selection of temporally separated time frames predicts intelligence. Notably, when selecting the same number of time frames as included previously in the selection of highest/lowest cofluctuation states (HiCo, LoCo), but ensuring their temporal separation – by selecting the 44 highest maxima (Mx) and lowest minima (Mn) across the entire cofluctuation time series – the prediction performance for intelligence increased markedly compared to the previous analyses. Specifically, the 44 highest maxima allowed us to reconstruct static functional connectivity on average with r = .93 (p < .001; Fig. 4a orange) and to significantly predict individual intelligence scores (r = .32, MAE = 9.75, all p < .001; Tab. 1, Fig. 4b orange dot). The same analyses based on a selection of the 44 lowest minima resulted in a reconstruction similarity of r =.66 (p < .001; Fig. 4a green) and also in significant prediction of intelligence, albeit with a lower prediction performance (r = .26, MAE = 10.09, all p < .01; Tab. 1, Fig. 4b green dot). Again, these results were similar for alternative prediction models, with CMEP showing robustly the best prediction results (Fig. S3).

To reveal the minimal amount of data necessary to predict individual differences in intelligence, we systematically varied the number of highest maxima and lowest minima time frames, respectively, and investigated how reconstruction similarity and prediction performances depend on this number. The ability to predict intelligence reached statistical significance at 20 time frames for the highest maxima (Fig. 4d) and at 27 time frames for the lowest minima (Fig. 4d). This result shows that individual intelligence scores can be predicted from as few as 20 time frames, equal to < 2.26% of a 10 min resting-state fMRI session (TR = 654ms, 884 TFs), as long as temporal independence of the selected time frames is ensured. These are considerably more time frames than necessary to reconstruct the static functional connectome (e.g., MxCo contained less than 14 frames), indicating that more independent data points are required to predict a complex human trait like general intelligence.

Randomly selected time frames predict intelligence as good as time frames of maximal cofluctuation. As states of highest maxima (Mx) are not significantly superior to states of lowest minima (Mn) in predicting intelligence (Fig. 4b), we next asked whether comparable prediction performances could be obtained when using an equal number of time frames randomly sampled from a uniform distribution over all time frames. Similar to the original HiCo and LoCo selections, also highest maxima (Mx) outperformed the randomly selected set of time frames in reconstructing the static connectivity matrix, whereas the lowest minima (Mn) performed significantly worse (orange and green line in comparison to the gray area in Fig. 4c). In contrast, when predicting intelligence, the random sets of time frames performed just as good as sets with an equal number of highest maxima (Fig. 4d). This suggests that while reconstruction similarity to the static FC primarily depends on the strength of cofluctuation, the prediction of intelligence is mainly determined by the number time frames.

Intelligence prediction involves multiple functional brain networks. The analyses reported so far used information from all possible functional brain connections for predicting intelligence. However, the brain can be decomposed into multiple non-overlapping networks (or modules) associated with different cognitive functions (e.g., 14). To assess their relative contributions to the prediction of intelligence, we repeated our analyses for a) static connectivity (all time frames) and b) the 44 highest maxima,

bioRxiv preprint doi: https://doi.org/10.1101/2022.12.23.521743; this version posted December 23, 2022. The copyright holder for this preprint (which was not certified by peer review) is the author/funder, who has granted bioRxiv a license to display the preprint in perpetuity. It is made available under aCC-BY-NC 4.0 International license.

considering seven established functional brain networks (38). Specifically, we analyzed, in a first step, the prediction performance of only the connections within a network and of those between a specific pair of networks. As illustrated in Fig. 5a, static connections linking the default-mode network to the dorsal attention network and to the fronto-parietal network for cognitive control significantly predicted intelligence ($p < .05$, Bonferroni corrected for 28 comparisons, i.e., 21 between-network analyses and 7 within-network analyses). When using the set of 44 highest maxima, only within-network connections (Fig. 5b) of the fronto-parietal network could significantly predict intelligence ($p < .05$, Bonferroni corrected for 28 comparisons). Secondly, we further explored the relevance of the seven functional networks for prediction of intelligence by analyzing the change in overall prediction performance when removing all connections, a specific network was involved in. For static connectivity removing one network only had a significant negative impact for the ventral attention network (Fig. 5c), whereas no significant changes in prediction performances were observed when analyzing the selection of 44 highest maxima (Fig. 5d; $p < .05$; both analyses Bonferroni corrected for seven repeated analyses, i.e., one per network). In sum, these results suggest that multiple functional brain systems – the attention networks, the fronto-parietal network, and the default mode network – contribute to the prediction of intelligence.

Robustness control analyses. Multiple control analyses were performed to further evaluate the robustness of our findings. As the choice of the cross-validation strategy can potentially influence the results of predictive modelling approaches (39), we first repeated our analyses for static functional connectivity and the 44 highest maxima using stratified 10-fold instead of LOO cross validation and obtained highly similar results (Tab. S1). Given that both the cognitive ability measure used in this study (FSIQ) and functional brain connectivity may vary with age (e.g., 40, 41) we secondly repeated our analyses using age-adjusted intelligence scores. As illustrated in Tab. S1, these analyses resulted in only a slight decrease in prediction performance but in overall comparable findings for static connectivity. In contrast, for the 44 highest maxima we observed a decrease in prediction performance suggesting that such states may vary stronger with age than the entire static connectivity matrix. Third, as functional connectivity estimates can be critically influenced by motion (e.g., 42, 43), we investigated whether there exists a temporal correspondence between the 44 highest maxima and high-motion time frames. This was not the case (Fig. S5a). Fourth, we tested whether the temporal distribution of the 44 highest maxima itself might be associated with variations in intelligence and observed that this also was not the case ($r = .05$, $p = .39$; Fig. S5b). In sum, the control analyses support the robustness of our findings.

External replication. Even though all of the results outlined above were thoroughly cross validated and tested for different confounding effects, potential remaining influences of sample-specific characteristics can only be ruled out by external replication (44). We therefore repeated our analyses using the four resting-state fMRI scans from the Human Connectome Project (HCP; $N = 831$, age range: 22 – 36 years; 100 nodes, 45; see Methods for details) each cropped to the same length as the time series of the primary sample (884 TFs). Given that the HCP data do not provide a full-scale IQ measure, general cognitive ability was operationalized as latent *g*-factor (46) computed from 12 cognitive performance scores (following 19; Fig. S1). This second dataset corroborated our prediction results (Tab. S2; Fig. S6): Static functional connectivity derived from all time frames could significantly predict intelligence (averaged across the four scans: $r = .27$, $p < .001$), while highest and lowest cofluctuation states could not (HiCo: $r = .08$, $p > .05$; LoCo: $r = .03$, $p > .05$). As in the primary dataset, restricting the selection to the maxima/minima during these highest/lowest cofluctuation states (< 17 TFs) resulted in only a slight decrease in reconstruction similarity (Tab. S2 in comparison to Tab. 1) and prediction performance (MxCo: $r = .07$, $p > .05$; MnCo: $r = .02$, $p > .05$). Finally, also in the replication sample, the 44 highest maxima and 44 lowest minima allowed for significant prediction of intelligence (Mx: $r = .23$, $p < .002$; Mn: $r = .14$, $p < .05$). Note that the reconstruction similarity to static connectivity was again highest in the latter cases (Mx: $r = .97$, Mn: $r = .75$). Finally, comparisons with randomly selected time frames and across increasing numbers of time frames resulted in similar findings as reported above for the original analyses (Fig. S6c,d).

Network-specific analyses in the replication sample yielded qualitatively similar findings, i.e., strong predictive power of connections linking the default mode, the fronto-parietal, and the attention networks

bioRxiv preprint doi: https://doi.org/10.1101/2022.12.23.521743; this version posted December 23, 2022. The copyright holder for this preprint (which was not certified by peer review) is the author/funder, who has granted bioRxiv a license to display the preprint in perpetuity. It is made available under aCC-BY-NC 4.0 International license.

(Fig. S7a,b). However, neither for static connectivity nor for the highest maxima state, those network-specific predictions reached statistical significance in the replication sample. Also, in no case prediction performance (MAE) decreased significantly when removing one network (all $p > .05$; Fig. S7c,d). While lacking the specificity observed in the primary sample, this supports the conclusion that multiple networks contribute to the prediction of intelligence. Lastly, an additional control analysis applying the 114-nodes Yeo-atlas used in the analyses of the primary data set to the replication sample yielded similar results and, thus, demonstrated the robustness of findings also against variations in different node parcellation schemes (Tab. S3). Overall, the results of the external replication support the generalizability of our findings to different samples, different scanning and preprocessing parameters, different age cohorts, and to different measures of general cognitive ability.

Discussion

Recent work has shown that brief states of particularly high functional connectivity reflect fundamental properties of individuals' functional connectomes measured across several minutes of resting-state fMRI (30, 31). Here, we explored whether these network-defining and person-specific states of high brain-wide cofluctuation – as well as other network states – carry information about individual differences in general cognitive ability (intelligence). We first replicated the basic phenomenon that the fundamental structure of static functional connectivity is driven by a small number of such high cofluctuation states (30). Further a machine learning-based prediction framework (CMEP) was developed to predict intelligence from functional connectivity created from only such states. However, neither the high cofluctuation states nor the states of particularly low cofluctuation were predictive for intelligence. This low prediction performance of high cofluctuation states as defined by (30) and (31) potentially results from the high number of temporally adjacent and thus correlated frames that carry little independent information. Secondly, we reveal that intelligence can be predicted from equally small selections of fMRI time frames – when such time frames are temporally independent. This holds true for selections of maxima and minima within the cofluctuation time series, as well as for random selections of time frames. Lastly, we show that intelligence can be predicted from selections of as few as 20 time frames, and that intelligence prediction relies on multiple functional brain networks, including the attention, fronto-parietal control, and the default mode systems. The replication of all results in an independent sample suggests generalizability of our findings to different populations, processing pipelines, and to various measures of cognitive ability.

How much brain data is required to predict human cognition? A large number of recent studies demonstrated that cognitive abilities can be predicted from functional brain connectivity measured with fMRI (20, 47). The recent advent of time-resolved brain connectivity analyses (30, 48) and of time-varying connectivity approaches in general (for review see 24) has made it possible to investigate the relationship between specific states of functional connectivity and cognition in more detail. Previous work has strongly focused on time frames of particularly high cofluctuation and demonstrated their ability to capture idiosyncratic information (31-33). In fact, our results suggest that the ability to predict intelligence is rather independent from the strength of cofluctuation but critically depends on the availability of sufficient independent data.

Further, our finding that prediction performance of intelligence increases with the number of time frames and that sufficient temporal independence is required, contradicts earlier studies proposing that scans as short as three to four minutes are sufficient to characterize individual subjects comprehensively (49, 50) and that even less than two minutes of resting-state fMRI can be used to build robust individual connectotypes (i.e., idiosyncratic connectivity properties; 51). In such short scanning durations, it might not be possible to detect a sufficient number of frames that contain enough independent trait-relevant information. On the one hand, our findings support the benefit of analyzing human brain connectivity with temporally fine-grained methods that prevent the temporal averaging step. On the other hand, we argue towards the relevance of longer scanning durations for neuroimaging research on individual differences in complex human traits to ensure capturing sufficient trait-relevant connectivity states.

Which brain states reflect individual differences in intelligence? While at the surface, our study asks for the smallest number of data points necessary to predict cognitive ability, the present research

bioRxiv preprint doi: https://doi.org/10.1101/2022.12.23.521743; this version posted December 23, 2022. The copyright holder for this preprint (which was not certified by peer review) is the author/funder, who has granted bioRxiv a license to display the preprint in perpetuity. It is made available under aCC-BY-NC 4.0 International license.

is primarily motivated by the aim of clarifying whether or not individual differences in intelligence depend upon specific brain states - as recently proposed by the Network Neuroscience Theory of Intelligence (NNT; 9). Identifying such connectivity states would not only open pathways for understanding the neurobiology underlying human cognition, but also reveal foci for treatment of cognitive diseases. We therefore defined a brain connectivity state as a selection of time frames from the fMRI connectivity time series that are all characterized by specific connectivity properties, and we probed such selections for their ability to predict individual intelligence scores.

The successful recovery of individual-specific connectomes from a limited number of high connectivity brain states (30) made these states a plausible first target. Ladwig and colleagues (52) suggested that focusing on time frames of higher cofluctuation increases the signal to noise ratio and thus increases the probability of detecting trait-relevant information. In contrast, in our study time frame selections with higher cofluctuation did not differ significantly from selections with lower cofluctuation regarding their predictive ability. This result is supported by (53), who find that lower and intermediate cofluctuation time frames provide higher subject specificity as well as highest phenotype predictions. Ladwig and colleagues (52) further demonstrated that high cofluctuation states are not necessarily special: removing these states from the connectivity time series did not impair the ability to derive individual connectomes, and random selections were equally capable of reconstructing static connectivity matrices. Relatedly, our result that even randomly selected time frames can predict intelligence as good as highest cofluctuation maxima suggests that intelligence-relevant information is not reflected in a specific brain-network organizational state (such as the high cofluctuation states) but is rather present in many fMRI time frames distributed across the entire scan. To summarize, intelligence does not seem to be characterized by a specific brain state, but rather by the ability of the human brain to explore different brain states over time.

Implications for understanding the brain bases of intelligence. The involvement of multiple functional brain networks in the prediction of intelligence from functional connectivity, observed here, is well in line with established neurocognitive theories of human intelligence (Parieto-Frontal Integration Theory, P-FIT, 54; Multiple Demand System, MD, 55) and more recent meta-analytic findings (5) suggesting that a widely distributed system of brain regions is implicated in individual differences in intelligence. Further support for the relevance of whole-brain analyses comes from a more theoretical perspective claiming that cognitively highly demanding activities – like complex problem solving – require the integration of information that is distributed widely across the brain (10). We observed particular relevance of the default-mode, the fronto-parietal, and the attention networks in the prediction of intelligence as well as the strongest reduction in prediction performance when removing the ventral attention network, corroborating previous results that these networks are especially relevant for individual differences in intelligence (e.g., 19, 20, 47; for review see 22). However, best predictions were achieved with whole-brain connectivity, highlighting the positive effect of information from all networks on predicting intelligence.

Introducing CMEP – a data-driven prediction framework for neuroscience. Finally, the here-introduced prediction framework - covariance maximizing eigenvector-based predictive modelling (CMEP) - has some notable advantages in comparison to previously used prediction methods for functional neuroimaging data. First, we demonstrated in multiple control analyses superior robustness of prediction results derived from CMEP in comparison to those derived from the to date most frequently used approach in network neuroscience (CPM; 20, 37). Second, CMEP is a completely data-driven framework, thereby making it unnecessary to (arbitrarily) select a threshold parameter (e.g., to identify most relevant brain connections). This reduces the researchers' degrees of freedom and thereby facilitates the reproducibility of results (56, 57). We therefore propose that CMEP is better suited to extract trait-like connectivity characteristics. However, compared to CPM, CMEP comes with slightly higher computational costs (1.14 x longer training time in comparison to CPM) and although the generated eigenvectors allow for more detailed functional interpretations (Fig. 2c), they produce more complex features than the two network averages used in CPM (i.e., a positive network and a negative network; cf. 20, 37). Despite these limitations, our results suggest CMEP as a promising candidate for broad applications in neuroscientific studies testing for brain-behavior relationships.

bioRxiv preprint doi: https://doi.org/10.1101/2022.12.23.521743; this version posted December 23, 2022. The copyright holder for this preprint (which was not certified by peer review) is the author/funder, who has granted bioRxiv a license to display the preprint in perpetuity. It is made available under aCC-BY-NC 4.0 International license.

Limitations and Future Directions. Our results are in line with the recent proposal in (9) that different brain states underly human cognition, however, we did not probe for the dynamic reconfiguration between such states. We have, however, recently demonstrated that persons with higher IQ scores show higher stability of network modularity over time – an effect that was in part driven by the same functional systems as identified here (8). These former results together with our current observation that even random selections of time frames allow for significant prediction of intelligence contradicts the NNT's proposal that the brain's ability to flexibly access a specific set of network states is essential for higher levels of intelligence (9). Whether higher network stability, higher network flexibility or neither of the two facilitates human cognition requires clarification in future work. However, our former study (8), the NNT (9), and our current findings all imply that individual differences in intelligence relate to the dynamic reconfigurations of functional connectivity over time, again highlighting the need for time-varying connectivity analyses and sufficient long scan durations.

The prediction performances in our study were in a comparable range to previous large-scale studies predicting intelligence or other complex human traits from static brain connectivity including all time frames (58; for review see 59) or even from brain structure (6; mean absolute error ~10 IQ points). However, it has recently been proposed that the investigation of brain-behavior relations requires large sample sizes (60-62) and that replication studies observe small effect sizes (Marek and colleagues found the largest 1% of replicable univariate effects to be between $|r| = .06$ and .16). Despite limited sample sizes in the range of hundreds our study demonstrates (via external validation) that the combination of cross-validation and sophisticated analyses approaches like CMEP allows to reliably identify brain-behavior associations - a promising direction for future research.

Conclusion. We introduced an eigenvector-based prediction framework to show that functional connectivity estimated from as few as 20 temporally separated time frames allow to significantly predict individual differences in general cognitive ability ($N = 281$). In contrast and against previous expectations, we revealed that network-defining time frames of particularly high or low cofluctuation are not predictive of intelligence, such that much more frames would be required to achieve a predictive performance comparable to the complete time series. Further we showed that multiple functional brain networks contribute to the prediction of cognitive ability from small selections of the fMRI time series, and all results replicate in an independent sample ($N = 831$). Overall, our results reveal that whereas relatively few time frames of brain connectivity are sufficient to derive fundamentals of person-specific functional connectomes, temporally distributed information and hence ultimately more data is necessary to extract information about cognitive abilities from functional connectivity time series. Importantly and in contrast to recent proposals, intelligence-predictive information is not restricted to specific brain connectivity states, but rather reflected within many different brain states that are temporally widely distributed over the whole brain connectivity time series. To detect such states requires sufficient amounts of neuroimaging data, making longer scanning durations essential for reliable prediction of complex human traits.

Materials and Methods

Participants

Primary sample

Data from the Enhanced NKI Rockland sample (NKI-RS Enhanced Sample; acquired by the Nathan S. Kline Institute for Psychiatric Research, Release 1-5; 35; RRID:SCR_010461) were used in all analyses. The NKI dataset was selected as primary sample, because a) participants were characterized by a well-established and reliable measure of intelligence (the Full Scale Intelligence Quotient/FSIQ; 34), which served as estimate of general cognitive ability, b) the sample is characterized by a broad variation in age and intelligence (in contrast to, e.g., to the Human Connectome Project; see Replication Sample), as it was explicitly recruited to be representative of the population, and c) because in addition to standard fMRI scanning protocols, fast-sampling resting-state fMRI data were also acquired, the temporal resolution of which is critical for the present study (see below for details). We restricted our analyses to subjects for whom complete fast-sampling fMRI data and IQ scores were available and which passed the Connectome Computational System (CCS) quality check (implying exact motion thresholds; see

bioRxiv preprint doi: https://doi.org/10.1101/2022.12.23.521743; this version posted December 23, 2022. The copyright holder for this preprint (which was not certified by peer review) is the author/funder, who has granted bioRxiv a license to display the preprint in perpetuity. It is made available under aCC-BY-NC 4.0 International license.

below). This resulted in a final sample of *N* = 281 participants (98 males, 246 right-handed, mean age: 47.19, 18 – 83 years; FSIQ: mean 101.44, range 69 – 141).

Replication sample

The generalizability of our findings to an independent sample is assessed with data from the Human Connectome Project (HCP; 1200 release; 36). After removing subjects with incomplete MRI data, missing phenotypic measures, or more than 10% motion spikes in the fMRI data (defined as framewise displacement, FD > .25 mm; see 63), the replication sample comprised *N* = 831 subjects (390 males, 756 right-handed, mean age: 28.55, 22 - 36 years). In contrast to the primary sample, the HCP dataset did not contain an intelligence test, but the Penn Matrix Test (PMAT) as a fast-to-administer approximation of fluid intelligence (64). PMAT scores represent the number of correct responses out of 24 items (mean 17.32, range 5 - 24 in our sample), but were not normally distributed in our sample (Shapiro-Wilk-Test: $W = .92$, $p < .001$). To construct a more comprehensive measure of general cognitive ability, we used 12 cognitive performance scores (65) to calculate a latent factor with bifactor analysis (19). Based on one of the most influential theories of intelligence (46), such a '*g*-factor' constitutes a valid representation of general cognitive ability. The standardized estimate of the *g*-factor (mean 0; range -3 – 2.32) was used as variable of interest for replication analyses.

All study procedures were approved by the NKI Institutional Review Board (#239708; primary sample), the Washington University Institutional Review Board (replication sample, for details see 36), and informed consent in accordance with the declaration of Helsinki was obtained from all participants.

Data acquisition and preprocessing

Primary sample

Fast sampling resting-state fMRI data (9:46 min; eyes open; TR = 654 ms, 884 time frames, voxel size = 3 mm isotropic, 40 slices, TE = 30 ms, flip angle = 60°, FOV = 222 x 222 mm^2) was obtained with a 32-channel head coil on a 3T Siemens Tim Trio scanner. A structural scan (T1-weighted, voxel size = 1 mm isotropic, 176 slices, TR = 1,900 ms, TE = 2.52 ms, flip angle = 9°, FOV = 250 × 250 mm^2) was acquired for coregistration. Data preprocessing was performed with the CCS pipeline (66; RRID:SCR_017342) and included discarding the first 16 volumes, removing outlier volumes (head motion, hardware instability), interpolation, slice time correction, motion correction, and global mean intensity normalization. Functional and structural scans were coregistered, nuisance variables (global, white matter, CSF mean signals and 24 motion parameters, i.e., six motion parameters of the current and the preceding scan, plus each of them squared; 67) were regressed out, data were temporally band-pass filtered (.01-.1 Hz), linear and quadratic trends were removed, and the resulting time-series were projected to MNI152 space. The CCS quality check was performed to identify anatomical images of low quality as well as subjects with a) mean FD > .2 mm, b) maximum translation > 3 mm, c) maximum rotation > 3°, or d) minimum cost of boundary-based registration > .6 (68). This led to the exclusion of 19 subjects from the initial sample of *N* = 300. Note that our method of using the CCS quality check for outlier removal (implemented via the 3dDespike AFNI function; 69, 70; https://afni.nimh.nih.gov/pub/dist/doc/program_help/3dDespike.htm; RRID:SCR_005927) is essentially equivalent to strict censoring (71, 72) or motion scrubbing (43), but replaces outlier time points via interpolation (72) instead of removing them. This ensures the same number of time points for all participants, which is especially important for analyses of functional connectivity dynamics (73, 74).

To construct functional connectivity matrices, brain volumes were parcellated into 114 regions of the Yeo atlas (38), which allow for the assignment of brain regions to seven functional networks: VIS, visual network; SMN, somatomotor network; DAN, dorsal attention network; VAN, ventral attention network; LIM, limbic network; CON, control network; DMN, default mode network. For each participant separately, functional connections were defined as weighted undirected edges and modelled using Fisher z-transformed Pearson correlation coefficients between the BOLD time series of each pair of brain regions (Fig. 1a). These edges represent brain connectivity as averaged across the whole duration of the resting-state scan and provide the basis for the construction of each participant's static connectivity matrix. In addition to the motion correction during preprocessing, we controlled for potential remaining

bioRxiv preprint doi: https://doi.org/10.1101/2022.12.23.521743; this version posted December 23, 2022. The copyright holder for this preprint (which was not certified by peer review) is the author/funder, who has granted bioRxiv a license to display the preprint in perpetuity. It is made available under aCC-BY-NC 4.0 International license.

influences of head motion by regressing out mean FD from each connectivity value with linear regression (http://scikitlearn.org/stable/modules/generated/sklearn.linear_model.LinearRegression.html).

Replication sample

Data of the replication sample consisted of the four resting-state runs from the HCP (15 min, 1,200 time points each; for details of data acquisition see 36). The scanning parameters were: voxel size = 2 mm isotropic, 72 slices, TR = 720 ms, TE = 33 ms, flip angle = 52°, FOV = 208 x 180 mm^2 (for details 75). We obtained the minimally preprocessed data from the HCP (76), involving an initial correction for head motion and B_0 distortion, co-registration to T1-weighted structural images, and normalization to MNI152 space. For further preprocessing, we followed strategy number six described in (63) (24HMP+8Phys+4GSR) which has been shown to perform well on the HCP resting-state data and maintains the same temporal degrees of freedom for all subjects. This strategy comprises regressing out a) 24 motion parameters including the raw scores as well as the squares of both the original and the derivate time series (77), b) eight physical parameters including white matter (WM) and cerebrospinal fluid (CSF) signals along with their temporal derivatives, squares, and squares of derivatives, and c) the global signal with its temporal derivative, square term, and the square of the derivatives. Also, a temporal band-pass filter of .008-.08 Hz was applied (63). Note that for comparability with the primary sample, i.e., to ensure same number of time frames, only 884 time frames in the center of the time series were used for further analyses. Brain volumes were parcellated into 100 regions of the Schaefer atlas (45), which allow direct alignment to the seven Yeo networks also used in the primary sample (38). Again, for each individual static (time-averaged) connectivity matrix, weighted edges were modelled on the basis of Fisher *z*-transformed Pearson correlation coefficients and remaining influences of head motion were controlled via regressing out mean FD and the number of spikes.

Time-resolved brain connectivity analyses. Following (30), we resolved connectivity in time to capture the strength of brain-wide cofluctuation for each time frame of the BOLD time series. Consider the Pearson correlation coefficient r_{ij} that reflects the time-averaged strength of interaction (functional connectivity) between two given nodes *i* and *j:*

$$r_{ij} = \frac{1}{T-1}\sum_{t=1}^{T} z_i(t)z_j(t) \quad (1)$$

where *T* is the number of fMRI time frames and $z_i(t)$ and $z_j(t)$ are the z-scored BOLD activity values at time *t* of nodes *i* and *j*, respectively. For example, for node *i*, the z-scored BOLD activity is defined as

$$z_i(t) = \frac{x_i(t) - \mu_i}{\sigma_i} \quad (2)$$

where $x_i(t)$ represents the BOLD activity at time *t*, μ_i is the mean of node i's time series, and σ_i is the respective standard deviation. The instantaneous cofluctuation between node i and node j at time frame *t* (representing time-resolved functional connectivity; Fig. 1b) is thus given by:

$$c_{ij}(t) = z_i(t)z_j(t) \quad (3)$$

On the basis of c_{ij}, we computed a three-dimensional time-resolved connectivity matrix for each participant (see Fig. 1c for a schematic illustration) with the shape *n* x *n* x *T*, where *n* is the number of nodes in the respective fMRI dataset (NKI: *n* = 114, HCP: *n* = 100) and *T* is the number of time frames (*T* = 884). The strength of *brain-wide* cofluctuation per time frame was then quantified by the root-sum-square (RSS; Fig 1e) of the cofluctuation values of all node pairs $c_{ij}(t)$ at a given time frame t:

$$RSS(t) = \sqrt{\sum_{i=1}^{n}\sum_{j=1}^{n} c_{ij}(t)^2} \quad (4)$$

bioRxiv preprint doi: https://doi.org/10.1101/2022.12.23.521743; this version posted December 23, 2022. The copyright holder for this preprint (which was not certified by peer review) is the author/funder, who has granted bioRxiv a license to display the preprint in perpetuity. It is made available under aCC-BY-NC 4.0 International license.

First, and in line with (30), we defined high cofluctuation states (also referred to as 'events') as those time frames with the 5% highest RSS values and low cofluctuation states as time frames with the 5% lowest RSS values, respectively (in our samples 44 time frames; Fig 1e, HiCo/LoCo, red and blue parts of the RSS curve). Second, as the temporally adjacent time frames included in these high and low cofluctuation states events are highly correlated with each other (for discussion see 52), we replaced each event of temporally grouped highest/lowest cofluctuation frames by the single frame with maximal/minimal cofluctuation within this event, thereby reducing the total number of frames considerably (Fig 1e, MxCo/MnCo, pink and light blue dots). Third, we selected from all maxima/minima within the *entire* RSS time series the 44 time frames with the overall highest/lowest cofluctuation values (again, 5% of data; Fig 1e, Mx/Mn, orange and green dots). Note that in the second and third case, but not in the first, the selected time frames were temporally separated from each other. For further analyses, and additionally to the previously computed static functional connectivity based on all time points (see above; Fig 1d), a functional connectivity matrix (Fisher z-transformed Pearson correlation, Fig. 1f) was computed from each of these six selected subsets of time frames (HiCo/LoCo, MxCo/MnCo, Mx/Mn), as well as for comparable random uniformly drawn subsets of time points. The resulting individual-specific functional connectivity matrices (seven per subject) were used as input to prediction analyses (Fig. 2).

Covariance maximizing eigenvector-based predictive modelling (CMEP). We developed a two-staged machine learning-based predictive modelling framework, which we refer to as covariance maximizing eigenvector-based predictive modelling (CMEP, see Fig. 2 for a schematic illustration). The basic idea of CMEP is to first create candidate features (based on eigenvectors) within a training set that share a strong linear relationship (covariance) with the target variable of interest, and then, in a second step, to assess the predictive power of these features by training and testing a prediction model (ElasticNet regression) based on these features. Notably, the ElasticNet regression circumvents the need to select features based on arbitrary threshold parameters (as is the case in many other prediction frameworks used for brain imaging data).

Feature construction

The key characteristic that differentiates CMEP from previous predictive modelling approaches is its feature construction method which amplifies features whose expression covary with a target variable (here intelligence). To this aim, functional connectivity matrices are projected into a scalar space chosen such that the covariation between individual intelligence scores and this scalar projection is maximal.

More specifically, within the training set, we find a projection ($\vec{u} \in \mathbb{R}^{nx1}$) that maximizes the covariance between intelligence scores ($q \in \mathbb{R}^{Nx1}$) and functional connectivity ($\boldsymbol{S} \in \mathbb{R}^{Nxnxn}$):

$$\underset{\vec{u}}{\operatorname{argmax}} \frac{1}{N}\sum_{p=1}^{N} \tilde{q}_p \vec{u}^{\mathrm{T}} \boldsymbol{S_p} \vec{u} \tag{5}$$

where $\tilde{q}_p$ represents the mean adjusted intelligence score, i.e., individual IQ (q_p) minus group-average IQ ($\bar{q}$) of a participant p. As the projection $\vec{u}$ is independent of p, Eq. 5 can be reformulated as follows

$$\underset{\vec{u}}{\operatorname{argmax}}\ \vec{u}^{\mathrm{T}} \left(\frac{1}{N}\sum_{p=1}^{N} \tilde{q}_p \boldsymbol{S_p} \right) \vec{u} \tag{6}$$

$$= \underset{\vec{u}}{\operatorname{argmax}}\ \vec{u}^{\mathrm{T}} \boldsymbol{M} \vec{u} \tag{7}$$

The matrix $\boldsymbol{M}$ (Fig. 2a,b) emphasizes intelligence-related differences in functional connectivity within the training set. Note that the leading eigenvector of $\boldsymbol{M}$ corresponds to the feature that maximally covaries with intelligence. However, it turned out that the prediction of general intelligence was more robust when

bioRxiv preprint doi: https://doi.org/10.1101/2022.12.23.521743; this version posted December 23, 2022. The copyright holder for this preprint (which was not certified by peer review) is the author/funder, who has granted bioRxiv a license to display the preprint in perpetuity. It is made available under aCC-BY-NC 4.0 International license.

including also other eigenvectors. Therefore, we next calculated the eigendecomposition of the general intelligence-weighted matrix $\boldsymbol{M}$:

$$\boldsymbol{M} = \boldsymbol{U}\boldsymbol{\Lambda}\boldsymbol{U}^{\mathrm{T}} \tag{8}$$

where $\boldsymbol{U}$ is the matrix of eigenvectors ($\boldsymbol{U} = [\overrightarrow{u_1}, \overrightarrow{u_2}, \dots, \overrightarrow{u_n}]$) and $\boldsymbol{\Lambda}$ is the diagonal matrix of the corresponding eigenvalues in decreasing order (Fig. 2c). We assumed that $\boldsymbol{M}$ is full rank and since it is real and symmetric, all eigenvalues are also real and the eigenvectors orthogonal. Note that the entries within a given eigenvector are interpretable as the weights of the corresponding nodes for that particular vector (Fig. 2c).

Then, subject-specific features are derived by projecting each participant's connectivity matrix $\boldsymbol{S_p}$ onto the previously computed eigenvectors $\overrightarrow{u_\iota}$:

$$\overrightarrow{u_\iota}^T \boldsymbol{S_p} \overrightarrow{u_\iota} = v_{pi} \tag{9}$$

This step results in an individual feature vector $\overrightarrow{v_p} = (v_{p1}, \dots, v_{pn}) \in \mathbb{R}^{nx1}$ for each participant *p* (Fig. 2d and f). The number of features is defined by the number of eigenvectors $\overrightarrow{u_\iota}$ and is thus equal to the number of nodes (n), i.e., 114 in the primary sample and 100 in the replication sample. Finally, an ElasticNet regression model is trained and optimized to predict intelligence scores from the generated feature vectors of an independent test set (Fig. 2e,f).

Prediction framework

The feature construction step of CMEP is embedded within a cross-validated prediction framework in which, within each cross-validation fold, a new set of eigenvector-based features are created to ensure strict independence between training and test set. Specifically, the prediction framework consists of two nested cross-validation loops. In the *outer* loop (primary sample: leave-one-subject-out cross validation; replication sample: leave-one-family-out due to family relations between participants) first, the eigenvectors $\boldsymbol{U}$ are computed from the training set. Second, the feature vectors $\overrightarrow{v_p}$ are constructed for each individual subject and third, an ElasticNet regression model is trained to predict the intelligence scores (q_p) from the subject-specific feature vectors ($\overrightarrow{v_p}$) within the training set. The hyperparameters of the ElasticNet model are optimized within the *inner* loop (5-fold cross-validation of the training set). ElasticNet regularizes a linear regression model via the L1 (Lasso; favoring feature sparsity) and L2 (Ridge; encouraging coefficient shrinkage) norm to avoid overfitting (78). Therefore, ElasticNet regression allows to utilize all created features as candidates for the prediction without manually setting an a-priori selection threshold. The model is formalized as:

$$argmin_\beta \sum_p \left(q_p - \sum_{j=1}^{n} \beta_j v_{pj} \right)^2 + \lambda_1 \sum_{j=1}^{n} |\beta_j| + \lambda_2 \sum_{j=1}^{n} \beta_j^2 \tag{10}$$

where β is the vector of regression weights and q_p and v_p are the cognitive ability score and the feature vector, respectively, of this specific participant. The hyperparameters λ_1 (L1-penalty) and λ_2 (L2-penalty) are optimized to minimize the mean squared error (MSE) between observed and predicted intelligence scores. The sklearn ElasticNetCV implementation in Python was used with parameter choices for $\alpha = \lambda_1 + \lambda_2 \in \{0.01, 0.02, 0.05, 0.1, 0.5, 1\}$, and L1-ratio = $\frac{\lambda_1}{\alpha} \in$ {0.01, 0.05, 0.1, $\frac{1}{3}$, 0.5, 0.7, 0.9, 0.95} to reduce computational costs. The obtained regression weights are then applied to the feature vector of the held-out subject (test set) to predict their intelligence score.

Prediction performance in terms of the difference between predicted and observed intelligence scores is evaluated using Pearson correlation coefficient (*r*), mean squared error (MSE), root mean squared error (RMSE), and mean absolute error (MAE). While MSE and RMSE capture differences in bias and

bioRxiv preprint doi: https://doi.org/10.1101/2022.12.23.521743; this version posted December 23, 2022. The copyright holder for this preprint (which was not certified by peer review) is the author/funder, who has granted bioRxiv a license to display the preprint in perpetuity. It is made available under aCC-BY-NC 4.0 International license.

precision, correlation coefficients and MAE can be more meaningfully interpreted and allow for direct comparability with previous reports (8).

Prediction robustness analyses

Three different control analyses were conducted with static (time-averaged) connectivity matrices to assess the validity of CMEP. Specifically, the robustness of prediction derived from CMEP were compared with those derived from the most frequently used neuroscientific prediction framework, i.e., connectome-based predictive modeling (CPM; 20). First, we assessed the robustness across different data set splits by randomly (100 times) dividing the data into 10 cross validation splits (Fig 3a). Second, to test the robustness across different samples sizes, the training sample was randomly (100 times) reduced to 10% of the original data size within each iteration of a stratified 10-fold cross-validation (Fig. 3b). Finally, the transferability of each model was assessed by training it on one sample (e.g., the primary sample, NKI) and testing it on an independent sample (e.g., the replication sample, HCP; Fig. 3c). To this end, both samples were parcellated into the 114 nodes partition and all intelligence scores were standardized. 100 different models were fitted, each with a randomly bootstrapped composition of the training set. All analyses described above were conducted four times, i.e., based on CMEP, the positive CPM network, the negative CPM network, and the combination of both, Specifically, in CPM prediction features are calculated as the sum over all functional connections that are significantly correlated with intelligence above a given threshold (here: $p < .001$; for details see 20, 37). Positively correlated connections were used to predict from a positive network, negatively correlated connections to predict from a negative network, and the positive and negative networks to predict from the whole brain.

Significance tests

Non-parametric permutation tests were used to assess the statistical significance of above-chance predictive model performance. Specifically, we took all N (primary sample: 281; replication sample: 831) target values (cognitive ability scores) and permuted them, which resulted in a random assignment between subjects and target values, and then assessed prediction performance (r, MSE, RMSE, MAE). This step was repeated 1,000 times. The significance of a model (p-value) was calculated as the fraction of times in which the permuted targets achieved a better model performance than the true targets. In cases where the prediction performance of two models was compared (see e.g., Fig. 5), a similar non-parametric procedure was adopted by comparing the difference in prediction performance between both models trained with the true targets and the difference in performance with permuted targets. Statistical significance was accepted for p values < .05.

bioRxiv preprint doi: https://doi.org/10.1101/2022.12.23.521743; this version posted December 23, 2022. The copyright holder for this preprint (which was not certified by peer review) is the author/funder, who has granted bioRxiv a license to display the preprint in perpetuity. It is made available under aCC-BY-NC 4.0 International license.

Acknowledgements

The authors thank the Nathan S. Kline Institute for Psychiatric Research (NKI; 35), founded and operated by the New York State office of mental health, for providing the primary data set for the current study, and the Human Connectome Project (36) for providing data of the replication sample. Finally, the authors thank Makoto Fukushima for providing the preprocessed NKI data.

Funding

The research leading to these results has received funding from the German Research Foundation (DFG Grant FI 848/6-1), the European Community's Seventh Framework Programme (FP7/2013) under Grant agreement n° 617891, and the Alfons and Gertrud Kassel-Stiftung (MW and MK). In part, the project was also supported by Lilly Endowment, Inc., through its support for the Indiana University Pervasive Technology Institute. KH received funding from the German Research Foundation (DFG Grant HI 2185/1-1).

Data Availability Statement

Data of the primary sample (NKI) can be accessed under http://fcon_1000.Projects.nitrc.org/indi/enhanced/. Data of the replication sample (HCP) can be downloaded from https://www.humanconnectome.org/study/hcp-young-adult. The analyses code for the preprocessing of the NKI sample can be obtained from https://github.com/zuoxinian/CCS and the analyses code for further preprocessing of the minimally preprocessed HCP data (replication sample) is available under https://github.com/faskowit/app-fmri-2-mat. Code of all further analyses (including CMEP) has been deposited on GitHub (https://github.com/kaschube-lab/CMEP).

bioRxiv preprint doi: https://doi.org/10.1101/2022.12.23.521743; this version posted December 23, 2022. The copyright holder for this preprint (which was not certified by peer review) is the author/funder, who has granted bioRxiv a license to display the preprint in perpetuity. It is made available under aCC-BY-NC 4.0 International license.

References

1. I. J. Deary, S. Strand, P. Smith, C. Fernandes, Intelligence and educational achievement. *Intelligence* **35**, 13-21 (2007).

2. T. Strenze, Intelligence and socioeconomic success: A meta-analytic review of longitudinal research. *Intelligence* **35**, 401-426 (2007).

3. G. D. Batty, I.J. Deary, Early life intelligence and adult health. *BMJ* **329**, 585 (2004).

4. A. Woolgar *et al.*, Fluid intelligence loss linked to restricted regions of damage within frontal and parietal cortex. *Proc. Natl. Acad. Sci. U.S.A.* **107***,* 14899–14902 (2010).

5. U. Basten, K. Hilger, C. J. Fiebach, Where smart brains are different: A quantitative meta-analysis of functional and structural brain imaging studies on intelligence. *Intelligence* **51**, 10-27 (2015).

6. K. Hilger *et al*., Predicting intelligence from brain gray matter volume. *Brain Struct Funct* **225** 2111-2129 (2020).

7. K. Hilger, M. Ekman, C. J. Fiebach, U. Basten, Efficient hubs in the intelligent brain: Nodal efficiency of hub regions in the salience network is associated with general intelligence. *Intelligence* **60**, 10-25 (2017).

8. K. Hilger, M. Fukushima, O. Sporns, C. J. Fiebach, Temporal stability of functional brain modules associated with human intelligence. *Hum Brain Mapp* **41**, 362-372 (2020).

9. A. K. Barbey, Network neuroscience theory of human intelligence. *Trends Cogn Sci* **22**, 8-20 (2018).

10. J. Duncan, M. Assem, S. Shashidhara, Integrated intelligence from distributed brain activity. *Trends Cogn Sci* **24**, 838-852 (2020).

11. G. T. Frischkorn, A. L. Schubert, D. Hagemann, Processing speed, working memory, and executive functions: Independent or inter-related predictors of general intelligence. *Intelligence* **75**, 95-110 (2019).

12. M. Euler, T. McKinney, "Evaluating the Weight of the Evidence: Cognitive Neuroscience Theories of Intelligence" in *The Cambridge Handbook of Intelligence and Cognitive Neuroscience,* A. Barbey, S. Karama, R. Haier, Eds. (Cambridge: Cambridge University Press, 2021) pp. 85-101.

13. K. Hilger, F. M. Spinath, S. Troche, A. L. Schubert, The biological basis of intelligence: Benchmark findings. *Intelligence* **93**, 101665 (2022).

14. M. D. Fox *et al.*, The human brain is intrinsically organized into dynamic, anticorrelated functional networks. *Proc. Natl. Acad. Sci. U.S.A.* **102**, 9673-9678 (2005).

15. M. D. Greicius, B. Krasnow, A. L. Reiss, V. Menon, Functional connectivity in the resting brain: a network analysis of the default mode hypothesis. *Proc. Natl. Acad. Sci. U.S.A.* **100**, 253-258 (2003).

16. W. W. Seeley *et al.*, Dissociable intrinsic connectivity networks for salience processing and executive control. *J Neurosci* **27**, 2349-2356 (2007).

17. O. Sporns, R. F. Betzel, Modular brain networks. *Annu Rev Psychol* **67***,* 613-640 (2016).

bioRxiv preprint doi: https://doi.org/10.1101/2022.12.23.521743; this version posted December 23, 2022. The copyright holder for this preprint (which was not certified by peer review) is the author/funder, who has granted bioRxiv a license to display the preprint in perpetuity. It is made available under aCC-BY-NC 4.0 International license.

18. B. Cai, *et al.,* Functional connectome fingerprinting: Identifying individuals and predicting cognitive function via deep learning. arXiv [Preprint] (2020). arXiv:2006.09928v1 (accessed 30 November 2022)

19. J. Dubois, P. Galdi, L. K. Paul, R. Adolphs, A distributed brain network predicts general intelligence from resting-state human neuroimaging data. *Philos Trans R Soc Lond B Biol Sci* **373**, 20170284 (2018).

20. E. S. Finn, *et al.*, Functional connectome fingerprinting: identifying individuals using patterns of brain connectivity. *Nat Neurosci* **18**, 1664-1671 (2015).

21. U. Pervaiz, D. Vidaurre, M. W. Woolrich, S. M. Smith, Optimising network modelling methods for fMRI. *Neuroimage* **211**, 116604 (2020).

22. K. Hilger, O. Sporns, "Network Neuroscience Methods for Studying Intelligence in *The Cambridge Handbook of Intelligence and Cognitive Neuroscience,* A. Barbey, S. Karama, R. Haier, Eds. (Cambridge: Cambridge University Press, 2021) pp. 26-43.

23. K. J. Friston, C. D. Frith, P. F. Liddle, R. S. J. Frackowiak, Functional connectivity: the principal-component analysis of large (PET) data sets. *J Cereb Blood Flow Metab* **13**, 5-14 (1993).

24. D. J. Lurie, *et al.*, Questions and controversies in the study of time-varying functional connectivity in resting fMRI. *Netw Neurosci* **4**, 30-69 (2020).

25. A. H. C. Fong, *et al.,* Dynamic functional connectivity during task performance and rest predicts individual differences in attention across studies. *Neuroimage* **188**, 14-25 (2019).

26. R. Jiang, *et al.,* Task-induced brain connectivity promotes the detection of individual differences in brain-behavior relationships. *Neuroimage* **207**, 116370 (2020).

27. I. Cifre, M. Zarepour, S. G. Horovitz, S. A. Cannas, D. R. Chialvo, Further results on why a point process is effective for estimating correlation between brain regions. *Pap Phys* **12**, 120003-120003 (2020).

28. E. Tagliazucchi, P. Balenzuela, D. Fraiman, D. R. Chialvo, Criticality in large-scale brain fMRI dynamics unveiled by a novel point process analysis. *Front Physiol* **3**, 15 (2012).

29. X. Liu, J. H. Duyn, Time-varying functional network information extracted from brief instances of spontaneous brain activity. *Proc. Natl. Acad. Sci. U.S.A.* **110**, 4392-4397 (2013).

30. F. Z. Esfahlani *et al.*, High-amplitude cofluctuations in cortical activity drive functional connectivity. *Proc. Natl. Acad. Sci. U.S.A.* **117**, 28393-28401 (2020).

31. R. F. Betzel, S. A. Cutts, S. Greenwell, J. Faskowitz, O. Sporns, Individualized event structure drives individual differences in whole-brain functional connectivity. *Neuroimage* **252**, 118993 (2022).

32. S. A. Cutts, J. Faskowitz, R. F. Betzel, O. Sporns, Uncovering individual differences in fine-scale dynamics of functional connectivity, *Cereb Cortex*, bhac214 (2022).

33. Olaf Sporns, Joshua Faskowitz, Andreia Sofia Teixeira, Sarah A. Cutts, Richard F. Betzel; Dynamic expression of brain functional systems disclosed by fine-scale analysis of edge time series. *Netw Neurosci* ***5***, 2 (2021).

bioRxiv preprint doi: https://doi.org/10.1101/2022.12.23.521743; this version posted December 23, 2022. The copyright holder for this preprint (which was not certified by peer review) is the author/funder, who has granted bioRxiv a license to display the preprint in perpetuity. It is made available under aCC-BY-NC 4.0 International license.

34. D. Wechsler, *Wechsler Abbreviated Scale of Intelligence* (Harcourt Brace and Company, 1999).

35. K. B. Nooner *et al.*, The NKI-Rockland sample: a model for accelerating the pace of discovery science in psychiatry. *Front Neurosci* **6**, 152 (2012).

36. D. C. Van Essen *et al.*, The WU-Minn human connectome project: an overview. *Neuroimage* **80**, 62-79 (2013).

37. X. Shen *et al.,* Using connectome-based predictive modeling to predict individual behavior from brain connectivity. *Nat Protoc* **12**, 506-518 (2017).

38. B. T. Yeo *et al.,* The organization of the human cerebral cortex estimated by intrinsic functional connectivity. *J Neurophysiol* **106**, 1125-1165 (2011).

39. G. Varoquaux, Cross-validation failure: Small sample sizes lead to large error bars. *Neuroimage* **180**, 68-77 (2018).

40. I. J. Deary *et al.,* Age-associated cognitive decline. *Brit med bull* **92**, 135-152 (2009).

41. L. Geerligs, R. J. Renken, E. Saliasi, N. M. Maurits, M. M. Lorist, A brain-wide study of age-related changes in functional connectivity. *Cereb cortex* **25**, 1987-1999 (2015).

42. R. Ciric *et al.,* Benchmarking of participant-level confound regression strategies for the control of motion artifact in studies of functional connectivity. *Neuroimage* **154**, 174-187 (2017).

43. J. D. Power, K. A. Barnes, A. Z. Snyder, B. L. Schlaggar, S. E. Petersen, Spurious but systematic correlations in functional connectivity MRI networks arise from subject motion. *Neuroimage* **59**, 2142–2154 (2012).

44. A. Cwiek *et al.,* Feeding the machine: Challenges to reproducible predictive modeling in resting-state connectomics. *Netw Neurosci* **6**, 29-48 (2022).

45. A. Schaefer *et al.,* Local-global parcellation of the human cerebral cortex from intrinsic functional connectivity MRI. *Cereb cortex* **28**, 3095-3114 (2018).

46. C. Spearman, General intelligence, objectively determined andmeasured. *Am J Psychol* **15**, 201–293 (1904).

47. J. Thiele, J. Faskowitz, O. Sporns, K. Hilger, Multi-Task Brain Network Reconfiguration is Inversely Associated with General Intelligence. *Cereb Cortex* **32***,* 1-11 (2022).

48. J. Faskowitz, F. Z. Esfahlani, Y. Jo, O. Sporns, R. F. Betzel, Edge-centric functional network representations of human cerebral cortex reveal overlapping system-level architecture. *Nat Neurosci* **23**, 1644-1654 (2019).

49. A. D. Airan *et al.,* Factors affecting characterization and localization of inter-individual differences in functional connectivity using MRI. *Hum Brain Mapp* **37**, 1986–1999 (2016).

50. L. Byrge, D. P. Kennedy *et al.,* High-accuracy individual identification using a “thin slice” of the functional connectome. *Netw Neurosci* **3**, 363-383 (2019).

51. O. Miranda-Dominguez *et al.,* Connectotyping: Model based fingerprinting of the functional connectome. PLoS One **9**, e111048 (2014).

bioRxiv preprint doi: https://doi.org/10.1101/2022.12.23.521743; this version posted December 23, 2022. The copyright holder for this preprint (which was not certified by peer review) is the author/funder, who has granted bioRxiv a license to display the preprint in perpetuity. It is made available under aCC-BY-NC 4.0 International license.

52. Z. Ladwig *et al.*, BOLD cofluctuation 'events' are predicted from static functional connectivity. *Neuroimage* **260**, 119476 (2022).

53. L. Sasse *et al.,* Intermediately Synchronised Brain States optimise trade-off between Subject Identifiability and Predictive Capacity. bioRxiv [Preprint] (2022). https://doi.org/10.1101/2022.09.30.510304 (accessed 1 December 2022).

54. R. E. Jung, P. J. Haier, The Parieto-Frontal Integration Theory (P-FIT) of intelligence: converging neuroimaging evidence. *Behav Brain Sci* **30**, 135-154 (2007).

55. J. Duncan, The multiple-demand (MD) system of the primate brain: mental programs for intelligent behaviour. *Trends Cogn Sci* **14**, 172–179 (2010).

56. R. O. Gilmore, M. T. Diaz, B. A. Wyble, T. Yarkoni, Progress toward openness, transparency, and reproducibility in cognitive neuroscience. *Ann NY Acad Sci* **1396**, 5-18 (2017).

57. R. A. Poldrack, The costs of reproducibility. *Neuron* **101**, 11-14 (2019).

58. T. He *et al.,* Deep neural networks and kernel regression achieve comparable accuracies for functional connectivity prediction of behavior and demographics. *Neuroimage* **206**, 116276 (2020).

59. A. S. Dizaji *et al.,* Linking Brain Biology to Intellectual Endowment: A Review on the Associations of Human Intelligence With Neuroimaging Data. *Basic ClinNeurosci* **12**, 1 (2021).

60. C. G. DeYoung *et al.,* Reproducible between-person brain-behavior associations do not always require thousands of individuals PryArXiv [Preprint] (2022). https://doi.org/10.31234/osf.io/sfnmk (accessed 1 December 2022).

61. M. D. Rosenberg, E. S. Finn, How to establish robust brain–behavior relationships without thousands of individuals. *Nat Neurosci* **25**, 835-837 (2022).

62. S. Marek *et al.,* Reproducible brain-wide association studies require thousands of individuals. *Nature* **603**, 654-660 (2022).

63. L. Parkes, B. Fulcher, M. Yücel, A. Fornito, An evaluation of the efficacy, reliability, and sensitivity of motion correction strategies for resting-state functional MRI. *Neuroimage* **171**, 415–436 (2018).

64. W. B. Bilker *et al.,* Development of abbreviated nine-item forms of the Raven's standard progressive matrices test. *Assessment* **19**, 354-369 (2012).

65. D. M. Barch *et al.,* Function in the human connectome: task-fMRI and individual differences in behavior. *Neuroimage* **80**, 169-189 (2013).

66. T. Xu, Z. Yang, L. Jiang, X. X. Xing, X. N. Zuo, A Connectome Computation System for discovery science of brain. *Sci Bull* **60**, 86–95 (2015).

67. K. J. Friston, S. Williams, R. Howard, R. S. Frackowiak, R. Turner, Movement-related effects in fMRI time-series. *Magn Reson Med* **35**, 346–355 (1996).

68. D. N. Greve, B. Fischl, Boundary based Registration. *Neuroimage* **48**, 63–72 (2010).

69. E. A. Allen *et al.,* Tracking whole-brain connectivity dynamics in the resting state. *Cereb Cortex,* **24**, 663–676 (2014).

bioRxiv preprint doi: https://doi.org/10.1101/2022.12.23.521743; this version posted December 23, 2022. The copyright holder for this preprint (which was not certified by peer review) is the author/funder, who has granted bioRxiv a license to display the preprint in perpetuity. It is made available under aCC-BY-NC 4.0 International license.

70. R. W. Cox, AFNI: what a long strange trip it's been. *Neuroimage* **62**, 743–747 (2012).

71. J. D. Power *et al.,* Methods to detect, characterize, and remove motion artifact in resting state fMRI. *Neuroimage* **84**, 320–341 (2014).

72. J. S. Siegel *et al.,* Data Quality Influences Observed Links Between Functional Connectivity and Behavior Data Quality In fluences Observed Links Between Functional Connectivity and Behavior. *Cereb Cortex* **27**, 4492-4502 (2017).

73. R. F. Betzel, M. Fukushima, Y. He, X. N. Zuo, O. Sporns, Dynamic fluctuations coincide with periods of high and low modularity in resting-state functional brain networks. *Neuroimage* **127**, 287–297 (2016).

74. M. Fukushima *et al.,* Fluctuations between high-and low-modularity topology in time-resolved functional connectivity. *Neuroimage* **180**, 406-416 (2018).

75. S. M. Smith *et al.,* Resting-state fMRI in the human connectome project. *Neuroimage* **80**, 144-168 (2013).

76. M. F. Glasser *et al.,* The minimal preprocessing pipelines for the Human Connectome Project. *Neuroimage* **80**, 105-124 (2013).

77. T. D. Satterthwaite *et al.,* An improved framework for confound regression and filtering for control of motion artifact in the preprocessing of resting-state functional connectivity data. *Neuroimage* **64**, 240–256 (2013).

78. H. Zou, T. Hastie, Regularization and variable selection via the elastic net. *J R Stat Soc Series B* **67**, 301–320 (2005).

Figures and Tables

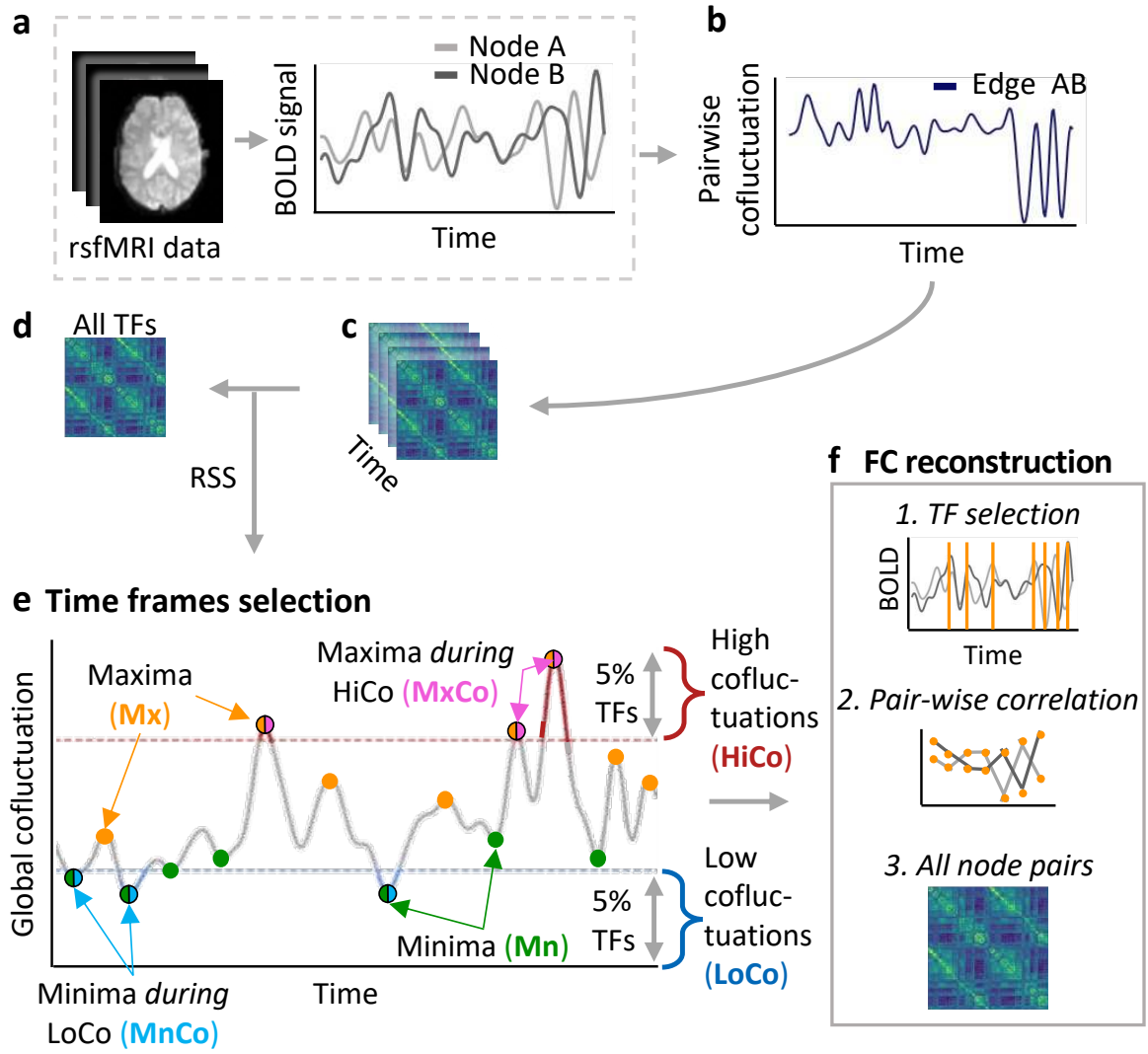

Figure 1. Schematic illustration of analysis steps to derive different types of state-restricted functional connectivity. (**a**) Resting-state fMRI data were parcellated into 114 functional brain regions (nodes; 38) and node-specific BOLD activation time courses were extracted. (**b**) For a given node pair, the strength of their cofluctuations is given by the product of their z-scored neural activation time series. Time-resolved whole-brain connectivity matrices (**c**) were then computed on the basis of all node-pairs instantaneous cofluctuation. Averaging this time-resolved connectivity matrices across all time frames (TFs) yields the full ('static') functional connectivity matrix (**d**). (**e**) The strength of instantaneous brain-wide (global) cofluctuation is computed as the root-sum-square (RSS) of all node-pair cofluctuations (30). Based on this *global* cofluctuation time series, six different brain connectivity states were defined (see Methods for details). The selections comprise i) the 44 time frames with the highest/lowest values of global cofluctuation (HiCo/LoCo), ii) only the maxima/minima within each of these short episodes of highest/lowest cofluctuation states (MxCo/MnCo, < 17 TFs) and iii) a larger set of, again, 44 time frames, but separated in time and representing the highest maxima/lowest minima within the complete RSS time series (maxima/minima, Mx/Mn). Apart from these specific selections of time frames, we also varied the number of frames and studied selections based on randomly drawn time-points. (**f**) On the basis of these different selections, functional connectivity matrices were computed as Fisher-z transformed Pearson correlation

representing the six subject-specific brain connectivity states. rsfMRI, resting-state functional magnetic resonance imaging.

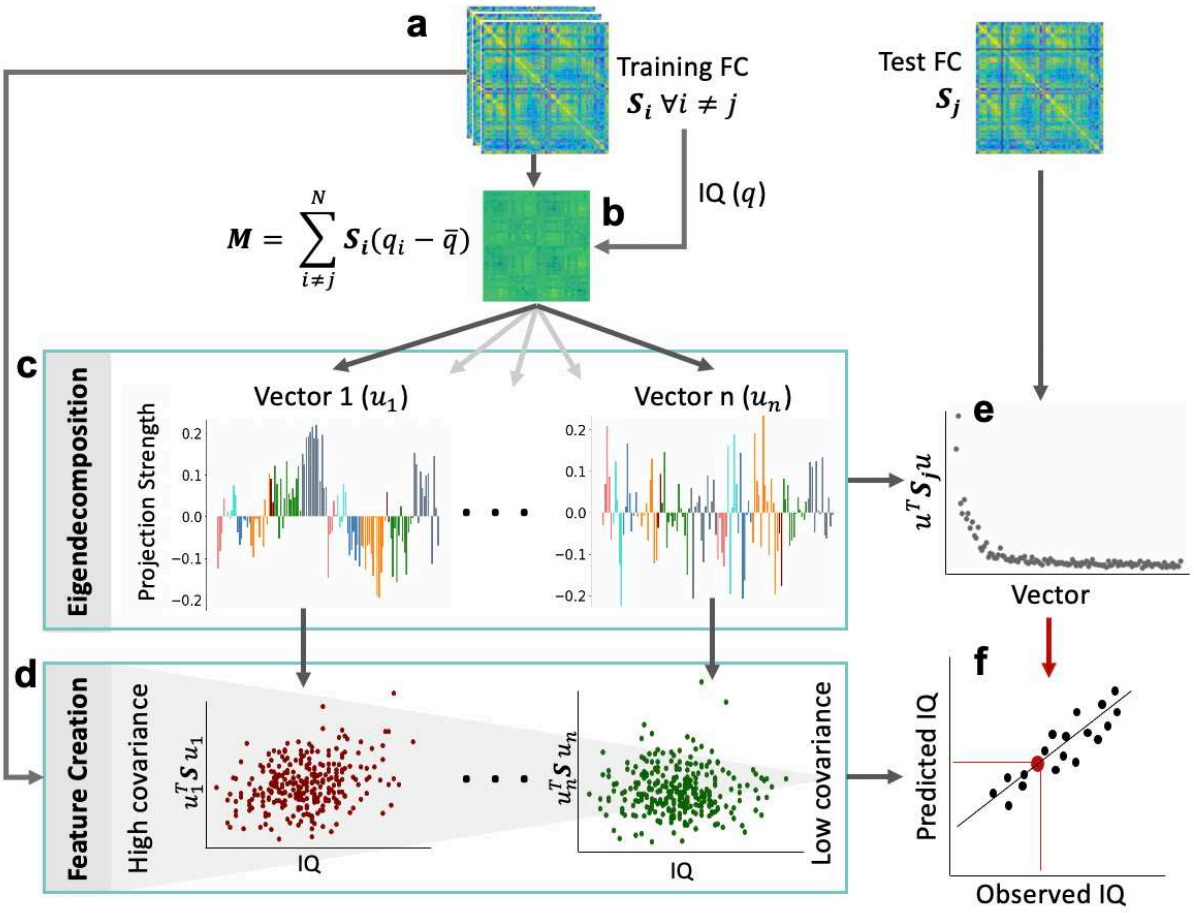

Figure 2: Schematic illustration of the Covariance Maximizing Eigenvector-Based Predictive Modelling (CMEP) framework. (**a**) For leave-one-out cross validation the functional connectivity ($\boldsymbol{S}$) was computed for every subject *i* and these data were split into a training and a test set. (**b**) Calculation of an IQ-weighted group connectivity matrix ($\boldsymbol{M}$) to enhance differences in intelligence-related features in the training sample. (**c**) Eigendecomposition of $\boldsymbol{M}$ generates the eigenvectors ($u_1 \ldots u_n$). The entries of the eigenvectors were highlighted in different colors according to the seven functional brain networks they correspond to (38; within each hemisphere; networks from left to right: visual, somatomotor, dorsal attention, ventral attention, limbic, control, and default mode). Projecting subject-specific functional connectivity onto these eigenvectors generates brain connectivity features for the training (**d**) and the left-out test sample (**e**). (**f**) All training set features were used to fit an ElasticNet regression and tested for generalization with the withheld test set features. Model performance was assessed by comparing the predicted with the observed intelligence scores. See Methods for further details.

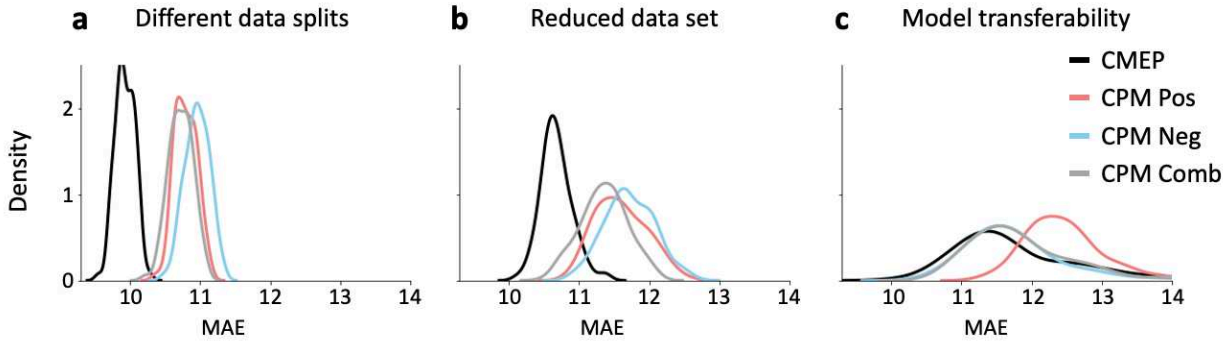

Figure 3. Superior prediction robustness of our method CMEP relative to connectome-based predictive modelling (CPM). Prediction performances (mean squared error, MAE, between observed and predicted intelligence scores) compared between CMEP and CPM based on static connectivity (using the entire time series) and three validity analyses (20, 37). All analyses were conducted for CMEP (black, all brain connections), and three CPM prediction pipelines based on positive connections (light red), negative connections (light blue), and a combination of both (light gray, all connections). (**a**) Robustness across different data set splits. Data were randomly (100 times) split into 10 folds for cross validation. (**b**) Robustness across different sample sizes. Within stratified 10-fold cross-validation, the training sample was randomly (100 times) reduced to 10% of the original sample size. (**c**) Transferability of the models to a new data set. Models were trained on the primary sample (NKI) and tested on the replication sample (HCP). Both samples were parcellated into the 114 nodes schemata (38) and all intelligence scores were standardized before prediction (but shown on original scale here for better comparability). The training data were randomly bootstrapped (100 times) to account for different compositions of the training data set.

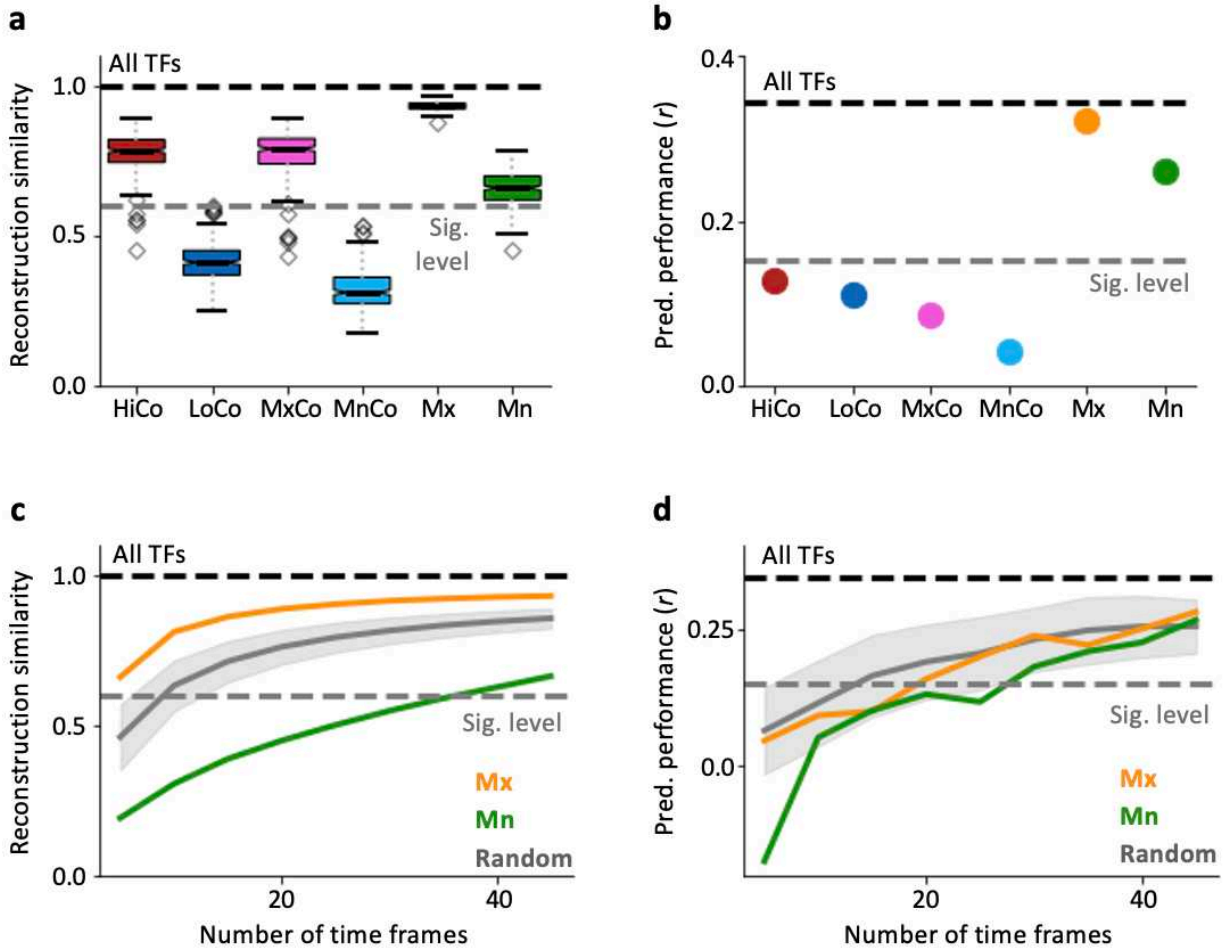

Figure 4. The performance to predict intelligence depends on the number of temporally separated time frames rather than on functional connectivity reconstruction similarity. (**a**) Reconstruction similarity of six different connectivity states operationalized as Pearson correlation between static functional connectivity (constructed from all time frames; TFs) and connectivity matrices reconstructed from six different selections of TFs (see Fig. 1). Boxplots depict the mean and quartiles of the subject-specific reconstruction similarity for all different connectivity states. The whiskers show the 1.5 x interquartile ranges. Outliers are represented by diamonds. (**b**) Prediction of intelligence (FSIQ; WASI, 34) for the six different connectivity states from using the CMEP prediction framework (see Fig. 2). (**c**) Reconstruction similarity and (**d**) performance to predict intelligence as a function of the number of time frames comprising cofluctuation maxima or cofluctuation minima (orange or green dots in Fig. 1e). Gray lines represent reconstruction similarity (**c**) and prediction performance (**d**) from randomly selected time frames (see Methods). Note that in (**c**) and (**d**) only the two cases are illustrated that allow for significant prediction of intelligence, i.e., 44 highest maxima, Mx; 44 lowest minima, Mn. The upper bounds (gray dashed lines) represent reconstruction similarity (**a, c**) or prediction performance (**b, d**) using all TFs. The lower grey dashed line reflects the 5% significance level of the within-subject similarity of static functional connectivity (**a, c**) or intelligence prediction performance (**b, d**) (see Methods). HiCo, highest cofluctuations; LoCo, lowest cofluctuations; MxCo, maxima during HiCo; MnCo, minima during LoCo; Mx, 44 highest maxima; Mn, 44 lowest minima (see also Fig. 1e).

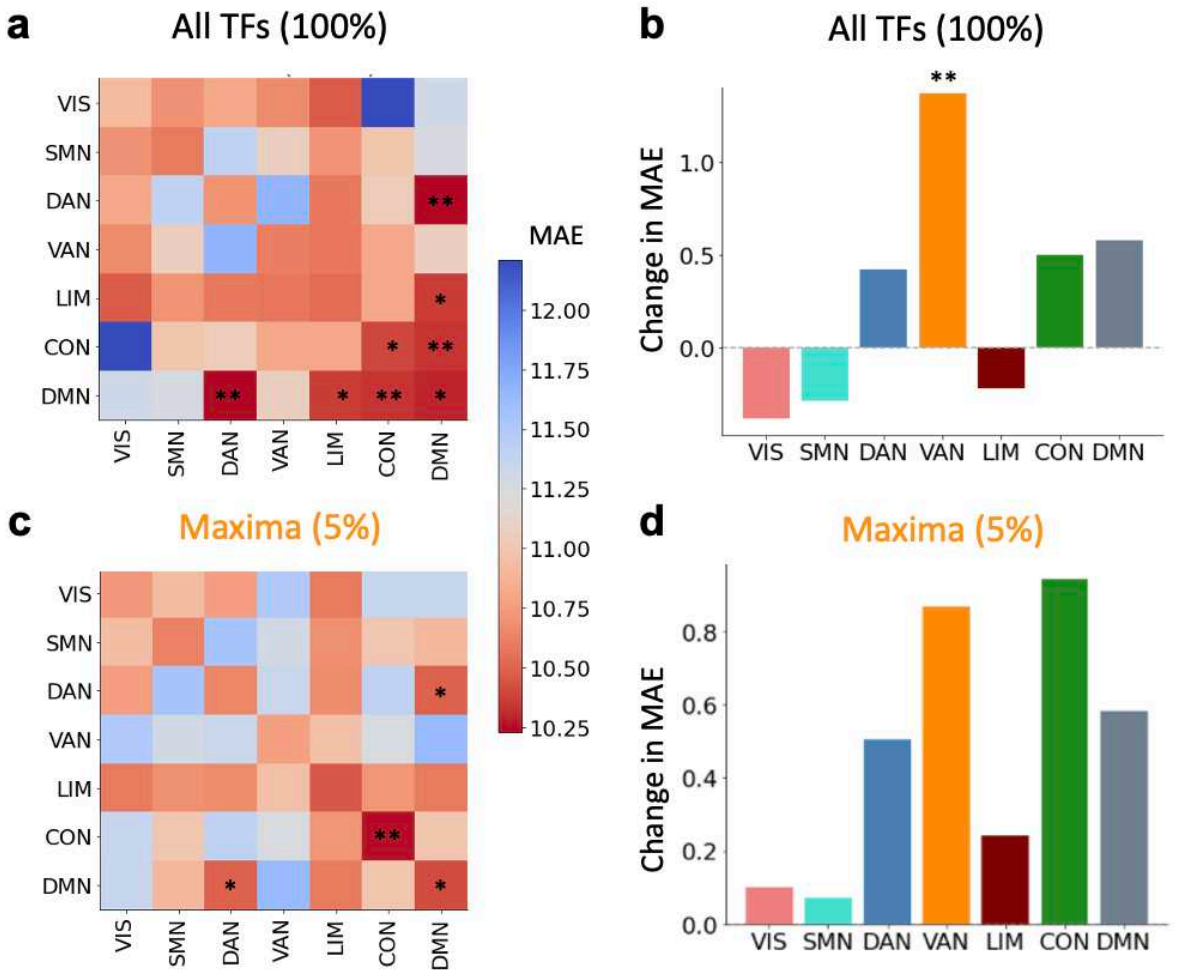

Figure 5. Multiple functional brain networks contribute to the prediction of intelligence. Intelligence (FSIQ; WASI, 34) was predicted with CMEP from (**a, b**) static functional connectivity (all time frames; TFs) and (**c, d**) from the 44 highest maxima of the global cofluctuation (Fig. 1e). In (**a, c**) prediction performance (mean absolute error; MAE) of connectivity within or between seven functional brain networks (38) was analyzed by selecting only the specific within or between network connections, while (**b, d**) illustrates the change in predictive performance (MAE) after removing all connections a respective network was involved in. Significance was determined by a non-parametric permutation test with 1,000 iterations. * if $p < .05$ uncorrected for multiple comparisons and ** if $p < .05$ Bonferroni corrected for multiple comparisons (28 comparisons, $p < .0018$ in a and **c** and seven comparisons, $p < .007$ in **b** and **d**). VIS, visual network; SMN, somatomotor network; DAN, dorsal attention network, VAN, ventral attention network; LIM, limbic network; CON, control network; DMN, default mode network.

Table 1. Prediction of intelligence from functional brain connectivity.

	TFs	Reconstruction similarity	*r*	MSE	RMSE	MAE
Static functional connectivity	884	n/a	.34**	155.97**	12.49**	9.84**
Highest cofluctuations (HiCo)	44	.78	.13	184.52	13.58	10.63
Lowest cofluctuations (LoCo)	44	.41	.11	179.13	13.38	10.40
Maxima during HiCo (MxCo)	7-14	.77	.09	183.21	13.54	10.65
Minima during LoCo (MnCo)	6-17	.32	.04	185.52	13.62	10.57
Highest maxima (Mx)	44	.93	.32**	158.73**	12.60**	9.75**
Lowest minima (Mn)	44	.66	.26**	165.57**	12.87**	10.09**

Note. Covariance maximizing eigenvector-based predictive modeling (CMEP; see Methods) was used in combination with a nested cross-validation scheme (see Methods, Fig. 1 and Fig. 2) to predict individual intelligence scores (Full Scale Intelligence Quotient, FSIQ; WASI, 34) from static connectivity (all fMRI time frames; TFs), highest and lowest cofluctuations (HiCo/LoCo; 44 TFs), maxima/minima during highest/lowes cofluctuation (MxCo/MnCo; < 17 TFs), and the 44 highest maxima and lowest minima across the whole RSS time series (Mx, Mn; see Methods and Fig. 1). Reconstruction similarity values represent Pearson correlations between the static connectivity matrix (row 1) and the reconstructed connectivity matrix from the respective selection of time frames. Model performance metrics reflect the error between predicted and observed intelligence scores: Pearson correlation coefficient (*r*), mean squared error (MSE), root mean squared error (RMSE), and mean absolute error (MAE). Significance was determined by a non-parametric permutation test with 1,000 iterations and indicated as ** if $p < .001$.

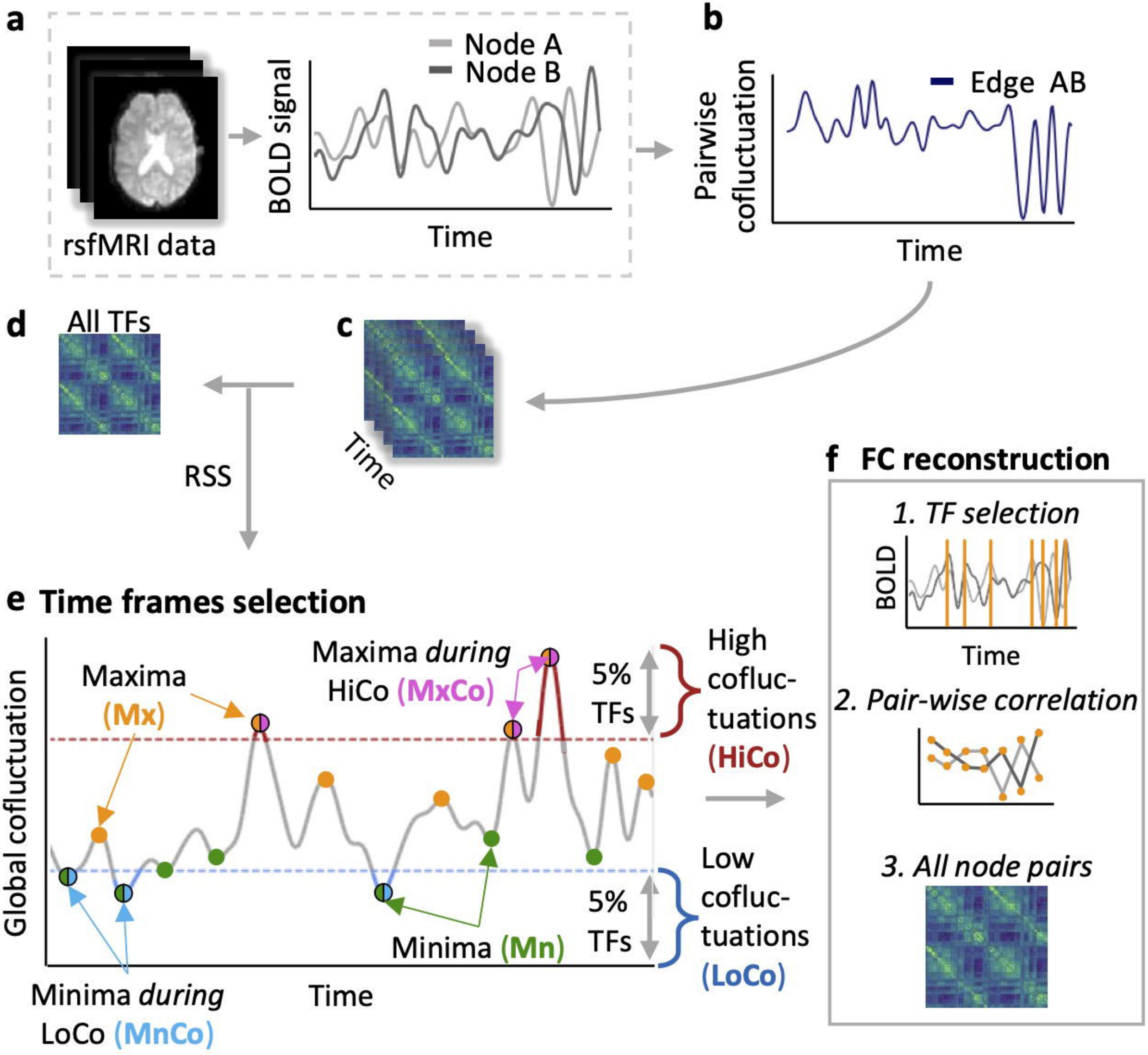
a
Node A
Node B
BOLD signal
Time
rsfMRI data
b
Pairwise cofluctuation
Edge AB
Time
c
Time
d
All TFs
RSS
e Time frames selection
Global cofluctuation
Maxima (Mx)
Maxima during HiCo (MxCo)
5% TFs
High cofluc-tuations (HiCo)
Minima (Mn)
5% TFs
Low cofluc-tuations (LoCo)
Minima during LoCo (MnCo)
Time
f FC reconstruction
1. TF selection
BOLD
Time
2. Pair-wise correlation
3. All node pairs

a

Training FC
$S_i \; \forall i \neq j$

Test
FC S_j

$$M = \sum_{i \neq j}^{N} S_i (q_i - \bar{q})$$

b

IQ (q)

c

Eigendecomposition

Projection Strength

0.2
0
-0.2

Vector 1 (u_1)

Vector n (u_n)

d

Feature Creation

High covariance

$u_1^T S u_1$

IQ

$u_n^T S u_n$

IQ

Low covariance

e

$u^T S_j u$

Vector

f

Predicted IQ

Observed IQ

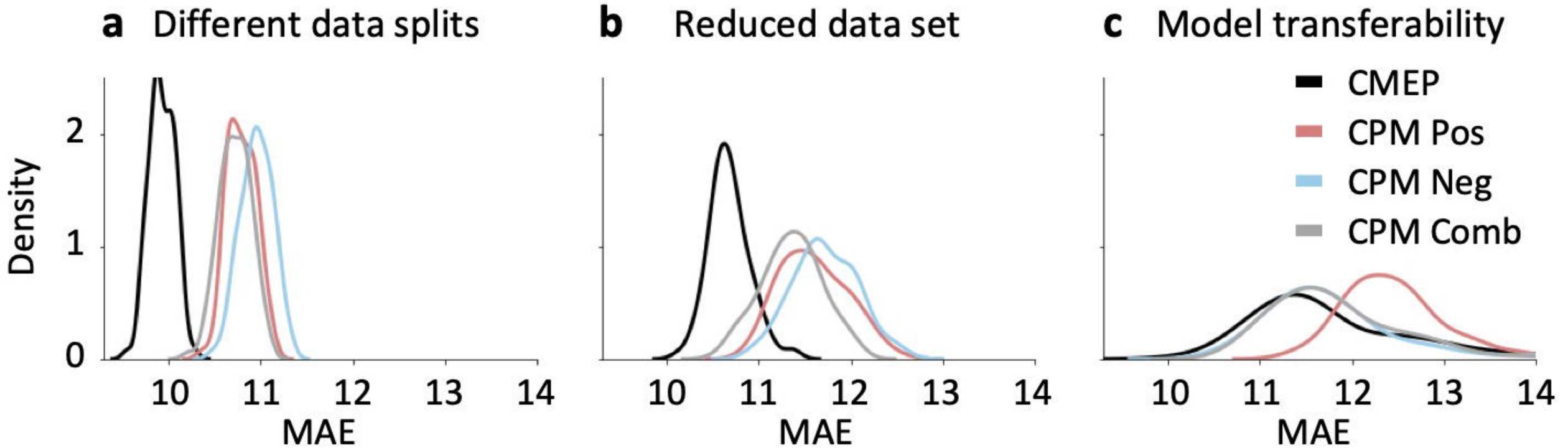
a Different data splits
b Reduced data set
c Model transferability
Density
0
1
2
10
11
12
13
14
MAE
CMEP
CPM Pos
CPM Neg
CPM Comb

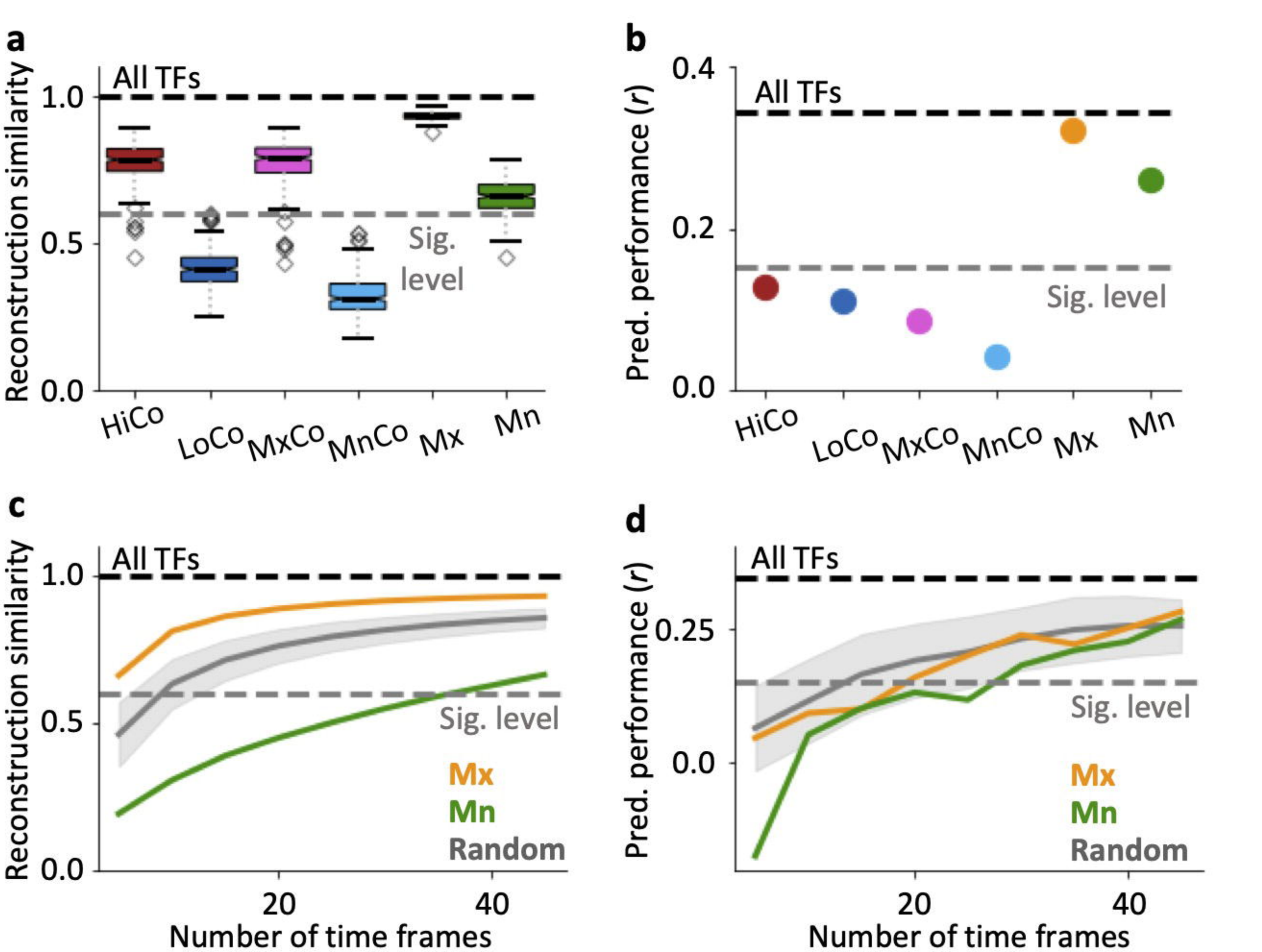
a
Reconstruction similarity
1.0
0.5
0.0
All TFs
Sig. level
HiCo
LoCo
MxCo
MnCo
Mx
Mn
b
Pred. performance (r)
0.4
0.2
0.0
All TFs
Sig. level
HiCo
LoCo
MxCo
MnCo
Mx
Mn
c
Reconstruction similarity
1.0
0.5
0.0
All TFs
Sig. level
Mx
Mn
Random
20
40
Number of time frames
d
Pred. performance (r)
0.25
0.0
All TFs
Sig. level
Mx
Mn
Random
20
40
Number of time frames

a All TFs (100%)

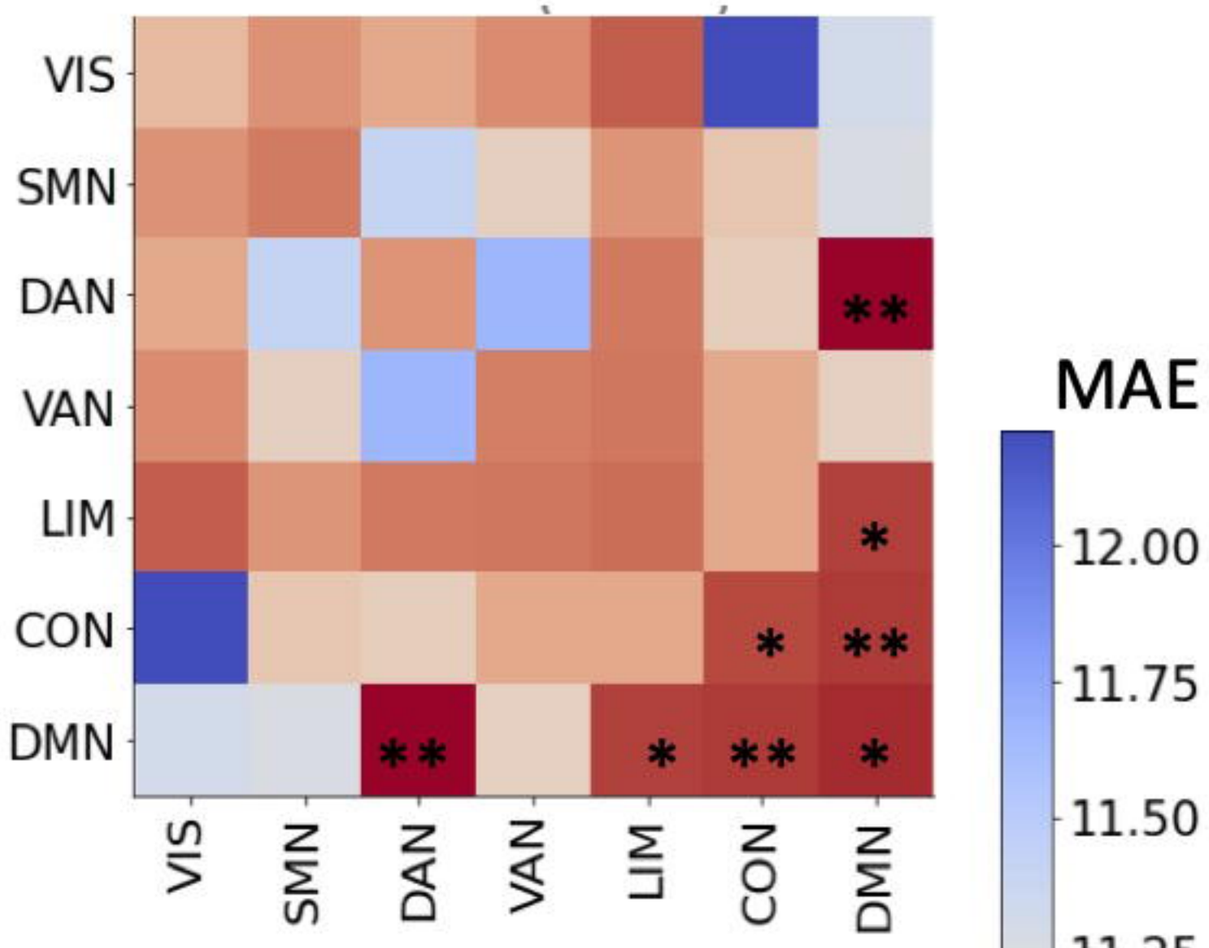

b All TFs (100%)

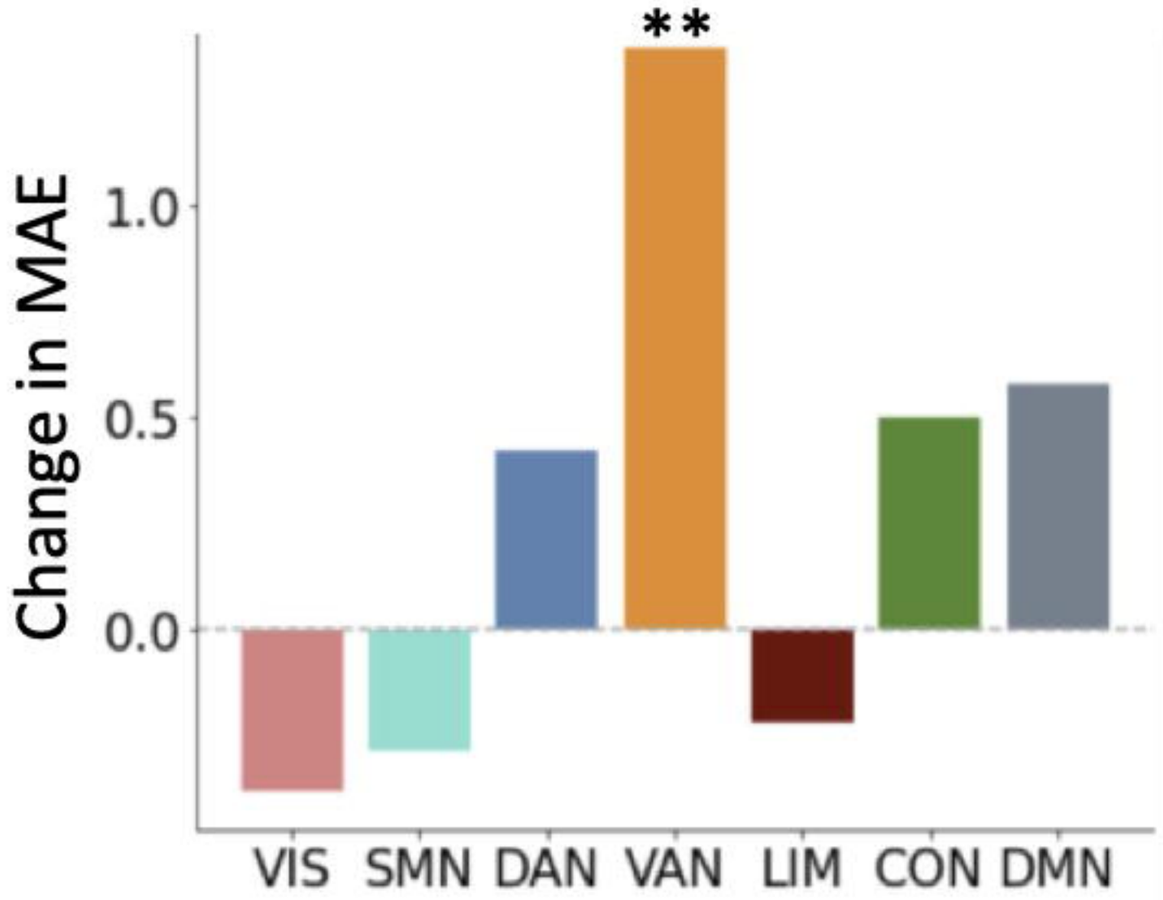

c Maxima (5%)

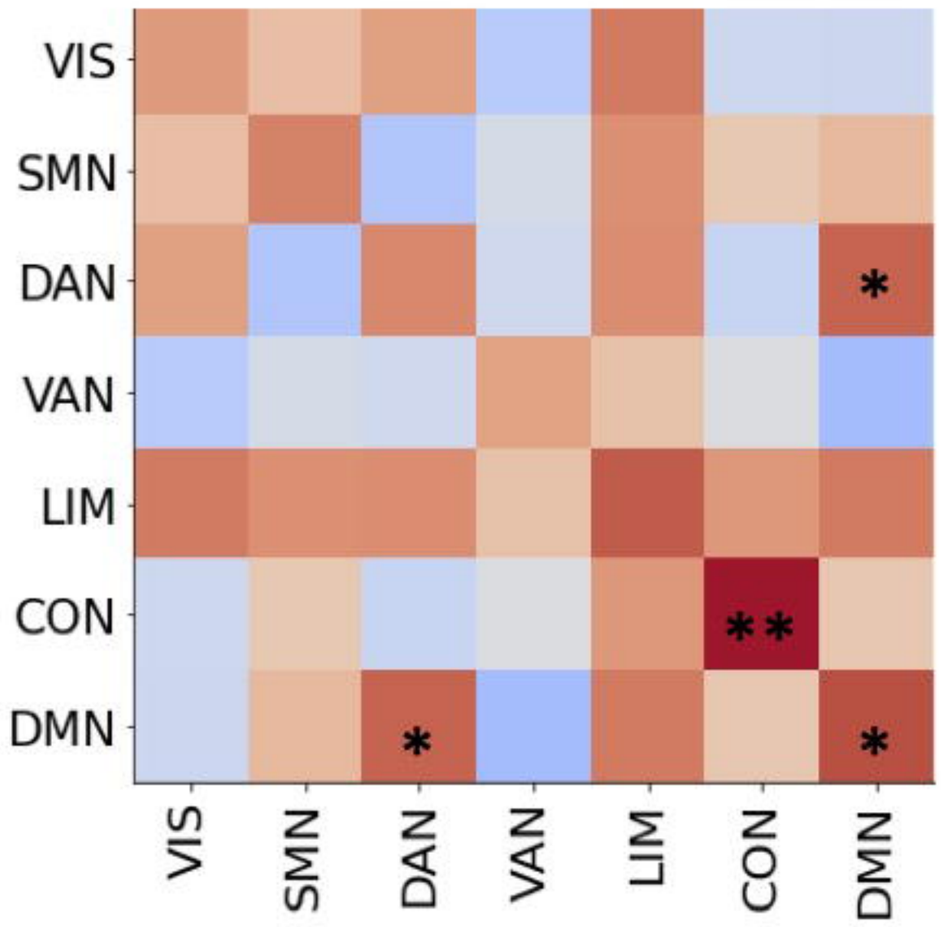

d Maxima (5%)